Continuum-kinematics-inspired peridynamics for transverse isotropy

A. M. de Villiers[a,*], J. Stadler[a], G. Limbert[b,c], A. T. McBride[d], A. Javili[e], P. Steinmann[f,d]

[a]*Applied Mathematics, Stellenbosch University, Private Bag X1. Matieland, 7602, South Africa*
[b]*Department of Mechanical Engineering, School of Engineering Sciences, Faculty of Engineering and Physical Sciences, University of Southampton, Southampton SO17 1BJ, United Kingdom*
[c]*Department of Human Biology, Faculty of Health Sciences, University of Cape Town, 7700 Cape Town, South Africa*
[d]*Glasgow Computational Engineering Centre, School of Engineering, University of Glasgow, Glasgow G12 8QQ, United Kingdom*
[e]*Department of Mechanical Engineering, Bilkent University, 06800 Ankara, Turkey*
[f]*Institute of Applied Mechanics, University of Erlangen-Nuremberg, Egerlandstr. 5, 91058 Erlangen, Germany*

Abstract

Accounting for the combined effects of mechanical anisotropy and nonlocality is critical for capturing a wide range of material behaviour. Continuum-kinematics-inspired peridynamics (CPD) provides the essential underpinning theoretical and numerical framework to realise this objective. The formalism of rational mechanics is employed here to rigorously extend CPD to the important case of transverse isotropy at finite deformations while retaining the fundamental deformation measures of length, area and volume intrinsic to classical continuum mechanics. Details of the anisotropic contribution to the potential energy density due to length, area and volume elements are given. A series of numerical examples serve to elucidate the theory presented.

Keywords: Peridynamics; Anisotropy; Nonlocal mechanics; Nonlinear kinematics; Rational mechanics.

1. Introduction

Transversely isotropic materials exhibit isotropic behaviour in a defined geometric plane and distinct properties orthogonal to it. Such directional dependence is present in many biological and engineered materials to achieve optimal performance. While the local (Cauchy) continuum theory for transversely isotropic materials undergoing finite deformations is well understood (see, e.g., Fu and Ogden, 2001; Holzapfel, 2000, and the references therein), this is not the case for the nonlocal continuum theory of peridynamics (PD) proposed by Silling (2000) (see Javili et al., 2019b, for a review of PD). The current study addresses this deficiency by extending the constitutive framework of continuum-inspired peridynamics (CPD) (Javili et al., 2019a) to account for the important case of transverse isotropy.

Classical local continuum theory lacks a length scale and thus cannot account for the size-dependent response exhibited by structures at small length scales. Extended continuum formulations, whose origins can be traced back to the work of Kröner (1967), address this deficiency. Eringen and co-workers (Eringen, 1972a,b, 1976; Eringen and Edelen, 1972) pioneered strongly nonlocal integral formulations where the stress at a material point depends on the weighted value of the strain in a finite neighbourhood. Conversely, weakly nonlocal gradient continuum theories (see, e.g., Gutkin and Aifantis, 1996; Kröner, 1967; Rogula, 1982; Vardoulakis et al., 1996) express the stress as a function of the strain and its gradients. Higher-order theories introduce additional degrees of freedom associated with

*Corresponding author.
Email address: andiedevilliers@sun.ac.za (A. M. de Villiers)

the microstructural response, with the most general being micromorphic theory (Eringen and Suhubi, 1964; Mindlin, 1964; Suhubi and Eringen, 1964).

The focus of this work is the strongly nonlocal continuum formulation of CPD (Javili et al., 2021a, 2019a, 2021b). Unlike the aforementioned nonlocal formulations, PD and CPD do not require the concepts of stress and strain. An appealing feature of CPD is its alignment with classical continuum mechanics, facilitating the formulation of transverse isotropy at finite deformations.

The motivation to account for anisotropy at finite deformations within a nonlocal continuum formulation is provided by a range of important phenomena. The macroscopic properties of fibre-reinforced composites emerge from the micro-scale interactions between fibres and the matrix, particularly as the size and aspect ratio of the reinforcing fibres vary (Asmanoglo and Menzel, 2017; Spencer and Soldatos, 2007). Steigmann (2012) provided a theoretical framework to predict such size-dependent behaviour, incorporating the impact of scale on stress distribution and failure mechanisms. Collectively, these studies reveal that the performance and structural integrity of fibre-reinforced composites are significantly influenced by size-dependent effects, necessitating a comprehensive approach to design and analysis that addresses the complex interplay between material size, fibre arrangement, and loading conditions. Soft biological tissues are endowed with anisotropic mechanical properties due to the presence of collagen fibres (see, e.g., Fung, 1993), and there is compelling experimental evidence that they exhibit multiple types of nonlocal behaviour ranging from non-affinity of deformation across length scales to long-range mechano-sensing and mechano-regulation of cells (Billiar and Sacks, 1997; Brewer et al., 2003; Hepworth et al., 2001; Krasny et al., 2017; Screen et al., 2004; Tower et al., 2002). Collagen fibres are hierarchical, featuring complex structural assemblies spanning multiple length scales. They interact with other elastic fibres (e.g., elastin), and the long-range mechanical interactions between the fibres and the surrounding matrix are complex. The mechanism of force transmission in such structures – fundamental to mechanobiology – can only be accurately described by non-local models.

Transverse isotropy has been accounted for by extending the original bond-based PD framework proposed in the seminal work of Silling (2000). In general, such extensions introduce a continuous relationship describing the variation in the physical and mechanical characteristics with respect to a preferred direction within the neighbourhood of a material points that then enters the force evaluation. This relationship typically reduces to scaling a material parameter within the neighbourhood using a simple (Hu et al., 2011, 2012) or more complicated function (Ghajari et al., 2014). In this spirit, Ahadi and Krochmal (2018) modulated the stiffness in the neighbourhood using an influence function that restricted interactions between neighbouring points to an ellipsoidal region. These models are restricted to bond-based peridynamics, where the Poisson's ratio is constrained, and infinitesimal deformations; overly restrictive assumptions for biological materials and engineered polymers.

State-based peridynamics (Silling et al., 2007) overcomes the key limitation of the original formulation. State-based PD was extended to account for transverse isotropy by Scabbia et al. (2024) using two bond stiffness functions, i.e., a single-bond micromodulus (which depends on the orientation of a single bond) and a double-bond micromodulus (which depends on the orientations of a pair of bonds). Other related works include Diana (2023); Li et al. (2024); Prakash (2022); Yang et al. (2024). The work on extending CPD to account for anisotropy is limited. Tian and Zhou (2021) introduced a linearised version of CPD that accounted for anisotropy based on the orientation of the vector formed by a one-neighbour interaction and the bi-sector formed by a two-neighbour interaction. Our previous work on a CPD formulation for elastoplasticity (Javili et al., 2021a) accounted for anisotropy in the plastic response via a direction-dependent yield function.

In this work, we present a novel generalised transverse isotropic constitutive model for finite elastic deformations

within the CPD framework. The constitutive model satisfies the essential requirements for material objectivity. The resulting numerical implementation is inherently stable. A series of numerical examples serve to elucidate the theory. Furthermore, enhanced modelling flexibility is achieved through area-element-based transverse anisotropy.

The structure of the presentation is as follows. Section 2 introduces the basic kinematics measures characterising CPD, i.e., line, area and volume elements, together with their transformations. Next, the internal potential energy for transverse anisotropy and the various contributions associated with line, area and volume elements are detailed in terms of invariants so as to satisfy the requirements of material objectivity. The resulting contributions to the governing equation are then outlined in Section 4, and the constitutive relations associated with line, area and volume elements highlighted, as well as directional influence functions that characterise anisotropic mechanical properties. Finally, a series of examples illustrate the versatility of the model and the ability to reproduce important physical behaviour.

2. Kinematics

Peridynamics is a non-local continuum formulation where each (infinitesimal) point in the material configuration $\mathcal{B}_0$ interacts with all other points within its horizon $\mathcal{H}_0$. The horizon is defined by a measure δ_0, that is typically the radius of a sphere. The position vector $\boldsymbol{X}$ indicates the location of a point in the material configuration. The nonlinear map $\boldsymbol{x} = \boldsymbol{y}(\boldsymbol{X})$ describes the motion of $\boldsymbol{X}$ to its position $\boldsymbol{x}$ in the spatial configuration $\mathcal{B}_t$. In the CPD framework (Javili et al., 2019a), the neighbour set of point $\boldsymbol{X}$ is identified as

$$\{\boldsymbol{X}^*\} = \{\boldsymbol{X}^* \,|\, \boldsymbol{X}^* \in \mathcal{H}_0\}\,, \tag{1}$$

where the superscript $*$ is a place holder to identify the neighbouring points within the horizon. The motion of each point in the neighbour set $\{\boldsymbol{X}^*\}$ to their respective position in the spatial configuration $\{\boldsymbol{x}^*\}$ is described by the nonlinear map $\boldsymbol{y}$, i.e., $\boldsymbol{x}^* = \boldsymbol{y}(\boldsymbol{X}^*)$. The kinematic response of a material point is described by the change in line-, area- and volume elements. These are respectively defined by the sets containing one-, two- and three-neighbour points, as indicated in Figure 1.

2.1. Line, area and volume elements

The relative position vector, or finite line element, between a point and its neighbour is denoted by $\boldsymbol{\Xi}^* := \boldsymbol{X}^* - \boldsymbol{X}$. The finite line element representing the relative deformation map is denoted by $\boldsymbol{\xi}^* := \boldsymbol{x}^* - \boldsymbol{x}$. These vectors can be respectively expressed in terms of their magnitudes, denoted by Ξ^* and ξ^*, and the material and spatial unit vectors, denoted by $\boldsymbol{E}^*$ and $\boldsymbol{e}^*$ (the rationale for this notation will be presented shortly):

$$\boldsymbol{\Xi}^* := |\boldsymbol{X}^* - \boldsymbol{X}|\, \boldsymbol{E}^* = \Xi^*\, \boldsymbol{E}^* \qquad \text{and} \qquad \boldsymbol{\xi}^* := |\boldsymbol{x}^* - \boldsymbol{x}|\, \boldsymbol{e}^* = \xi^*\, \boldsymbol{e}^*\,. \tag{2}$$

A one-neighbour interaction considers the line element between a point $\boldsymbol{X}$ and one of its neighbours $\boldsymbol{X}^|$. The set of one-neighbours that forms these bonds are denoted $\{\boldsymbol{X}^| \,|\, \boldsymbol{X}^| \in \{\boldsymbol{X}^*\}\}$. The bond stretch captures the deformation of the line element as follows

$$\lambda^| := \xi^| / \Xi^| > 0\,. \tag{3}$$

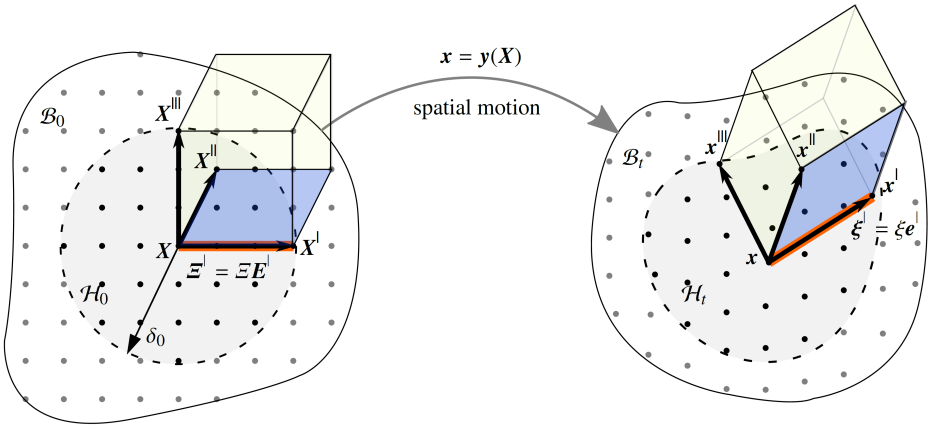

Figure 1: Motion of a continuum body in the CPD framework

A two-neighbour interaction considers the area element formed by the point $\boldsymbol{X}$ and two of its neighbours, $\boldsymbol{X}^{I}$ and $\boldsymbol{X}^{II}$. The set of two-neighbours that forms these double-bonds is denoted $\{\boldsymbol{X}^{I}, \boldsymbol{X}^{II} \,|\, \boldsymbol{X}^{I}, \boldsymbol{X}^{II} \in \{\boldsymbol{X}^{*}\}\}$. The vectorial area elements $\boldsymbol{\Xi}^{I/II}$ and $\boldsymbol{\xi}^{I/II}$ in the material and spatial configurations, respectively, can be expressed in terms of their magnitudes, $\Xi^{I/II}$ and $\xi^{I/II}$, and unit vectors perpendicular to their area element, $\boldsymbol{E}^{I/II}$ and $\boldsymbol{e}^{I/II}$, as

$$\begin{aligned} \boldsymbol{\Xi}^{I/II} &:= |\boldsymbol{\Xi}^{I} \times \boldsymbol{\Xi}^{II}|\, \boldsymbol{E}^{I/II} = \Xi^{I/II}\, \boldsymbol{E}^{I/II} && \text{with} && \boldsymbol{E}^{I/II} = \frac{\boldsymbol{\Xi}^{I} \times \boldsymbol{\Xi}^{II}}{|\boldsymbol{\Xi}^{I} \times \boldsymbol{\Xi}^{II}|}\,, \\ \boldsymbol{\xi}^{I/II} &:= |\boldsymbol{\xi}^{I} \times \boldsymbol{\xi}^{II}|\, \boldsymbol{e}^{I/II} = \xi^{I/II}\, \boldsymbol{e}^{I/II} && \text{with} && \boldsymbol{e}^{I/II} = \frac{\boldsymbol{\xi}^{I} \times \boldsymbol{\xi}^{II}}{|\boldsymbol{\xi}^{I} \times \boldsymbol{\xi}^{II}|}\,. \end{aligned} \tag{4}$$

The double-bond stretch captures the deformation of the area element associated with a two-neighbour interaction and is denoted by

$$\lambda^{I/II} := \xi^{I/II} / \Xi^{I/II} > 0\,. \tag{5}$$

A three-neighbour interaction considers the volume element formed by the point $\boldsymbol{X}$ and three neighbours, $\boldsymbol{X}^{I}, \boldsymbol{X}^{II}$, and $\boldsymbol{X}^{III}$. The set of three-neighbours that forms these triple-bonds is denoted $\{\boldsymbol{X}^{I}, \boldsymbol{X}^{II}, \boldsymbol{X}^{III} \,|\, \boldsymbol{X}^{I}, \boldsymbol{X}^{II}, \boldsymbol{X}^{III} \in \{\boldsymbol{X}^{*}\}\}$. The signed scalar-valued volume elements $\boldsymbol{\Xi}^{I/II/III}$ and $\boldsymbol{\xi}^{I/II/III}$ are written in terms of their magnitudes $\Xi^{I/II/III}$ and $\xi^{I/II/III}$ as

$$\boldsymbol{\Xi}^{I/II/III} := \pm \left| \left[\boldsymbol{\Xi}^{I} \times \boldsymbol{\Xi}^{II} \right] \cdot \boldsymbol{\Xi}^{III} \right| = \Xi^{I/II/III}\, \boldsymbol{E}^{I/II/III} \quad \text{and} \quad \boldsymbol{\xi}^{I/II/III} := \pm \left| \left[\boldsymbol{\xi}^{I} \times \boldsymbol{\xi}^{II} \right] \cdot \boldsymbol{\xi}^{III} \right| = \xi^{I/II/III}\, \boldsymbol{e}^{I/II/III}\,. \tag{6}$$

Here the notation $\boldsymbol{e}^{I/II/III}$ and $\boldsymbol{E}^{I/II/III}$ refers to the signed scalar (see Remark 1 below). That is,

$$\boldsymbol{E}^{I/II/III} = \frac{\left[\boldsymbol{E}^{I} \times \boldsymbol{E}^{II} \right] \cdot \boldsymbol{E}^{III}}{\left| \left[\boldsymbol{E}^{I} \times \boldsymbol{E}^{II} \right] \cdot \boldsymbol{E}^{III} \right|} = \pm 1 \qquad \text{and} \qquad \boldsymbol{e}^{I/II/III} = \frac{\left[\boldsymbol{e}^{I} \times \boldsymbol{e}^{II} \right] \cdot \boldsymbol{e}^{III}}{\left| \left[\boldsymbol{e}^{I} \times \boldsymbol{e}^{II} \right] \cdot \boldsymbol{e}^{III} \right|} = \pm 1\,. \tag{7}$$

The triple-bond stretch (or volume change) captures the deformation of the volume element associated with a three-

neighbour interaction and is denoted by

$$\lambda^{\mathrm{I}/\mathrm{II}/\mathrm{III}} := \xi^{\mathrm{I}/\mathrm{II}/\mathrm{III}} / \Xi^{\mathrm{I}/\mathrm{II}/\mathrm{III}} > 0\,. \tag{8}$$

Remark 1. A boldface symbol typically denotes a vector or a tensor. The exception is that signed scalars associated with the kinematic measures of volume elements are also boldface. □

2.2. Linear transformation of line, area and volume elements

The three fundamental kinematic measures from classical continuum mechanics (CCM) are the deformation gradient $\boldsymbol{F}$, its cofactor $\boldsymbol{K}$ and its determinant J. These represent linear transformations of an *infinitesimal* line element $\mathrm{d}\boldsymbol{X}$, an *infinitesimal* area element $\mathrm{d}\boldsymbol{A}$ and an *infinitesimal* volume element $\mathrm{d}V$ from the material configuration to their counterparts, $\mathrm{d}\boldsymbol{x}$, $\mathrm{d}\boldsymbol{a}$ and $\mathrm{d}v$, respectively, in the spatial configuration. In CPD, these kinematic measures are mimicked by linear transformations of the *finite* line, area and volume elements characterising one-neighbour, two-neighbour and three-neighbour interactions, respectively. The bond-based *secant* map $\mathbb{F}^{\mathrm{I}}$ linearly transforms a *finite* line element $\boldsymbol{\Xi}^{\mathrm{I}}$ from the material configuration to their counterpart in the spatial configuration $\boldsymbol{\xi}^{\mathrm{I}}$ as follows

$$\boldsymbol{\xi}^{\mathrm{I}} = \mathbb{F}^{\mathrm{I}} \cdot \boldsymbol{\Xi}^{\mathrm{I}} \qquad \text{with} \qquad \mathbb{F}^{\mathrm{I}} := \lambda^{\mathrm{I}} \boldsymbol{e}^{\mathrm{I}} \otimes \boldsymbol{E}^{\mathrm{I}}\,. \tag{9}$$

Similarly, the *double-bond based co-secant map* $\mathbb{F}^{\mathrm{I}/\mathrm{II}}$ linearly transforms *finite* area elements from the material to the spatial configuration as

$$\boldsymbol{\xi}^{\mathrm{I}/\mathrm{II}} = \mathbb{F}^{\mathrm{I}/\mathrm{II}} \cdot \boldsymbol{\Xi}^{\mathrm{I}/\mathrm{II}} \qquad \text{with} \qquad \mathbb{F}^{\mathrm{I}/\mathrm{II}} := \lambda^{\mathrm{I}/\mathrm{II}} \boldsymbol{e}^{\mathrm{I}/\mathrm{II}} \otimes \boldsymbol{E}^{\mathrm{I}/\mathrm{II}}\,. \tag{10}$$

Finally, *finite* volume elements are mapped by the *triple-bond based volume measure map* $\mathbb{F}^{\mathrm{I}/\mathrm{II}/\mathrm{III}}$ as

$$\boldsymbol{\xi}^{\mathrm{I}/\mathrm{II}/\mathrm{III}} = \mathbb{F}^{\mathrm{I}/\mathrm{II}/\mathrm{III}}\, \boldsymbol{\Xi}^{\mathrm{I}/\mathrm{II}/\mathrm{III}} \qquad \text{with} \qquad \mathbb{F}^{\mathrm{I}/\mathrm{II}/\mathrm{III}} := \lambda^{\mathrm{I}/\mathrm{II}/\mathrm{III}}\, \boldsymbol{e}^{\mathrm{I}/\mathrm{II}/\mathrm{III}}\, \boldsymbol{E}^{\mathrm{I}/\mathrm{II}/\mathrm{III}}\,. \tag{11}$$

Remark 2. Unlike the bond-based secant map and the double-bond based co-secant map, which transform vectors, the triple-bond based material measure map describes a scalar transformation and should be interpreted as a volume ratio. This corresponds to $J := \mathrm{Det}\boldsymbol{F}$ in CCM. Only for affine deformations, i.e., in the local limit ($\delta \to 0$), do the relations between $\boldsymbol{F}$, its cofactor $\boldsymbol{K}$ and its determinant J hold for the otherwise independent linear mappings in Eqs. (9)-(11). □

3. Internal potential energy for transverse anisotropy

For elastic deformations, the governing equations for a body can be obtained by minimising its total potential energy functional $\mathcal{E}$, i.e., finding equilibrium by requiring $\delta\mathcal{E} \doteq 0 \,\forall\, \delta\boldsymbol{y}$. The total energy consists of internal and external contributions. The internal potential energy $\mathcal{E}^{\mathrm{int}}$ is the stored energy Ψ in the body, i.e., $\mathcal{E}^{\mathrm{int}} = \Psi$. In CPD the stored energy is composed of contributions from line elements, area elements and volume elements as

$$\Psi = \Psi_1 + \Psi_2 + \Psi_3\,. \tag{12}$$

For simplicity, external contributions will be neglected and equilibrium implies that

$$\delta\Psi \doteq 0 \quad \forall\, \delta\boldsymbol{y} \qquad \Rightarrow \qquad \delta\Psi_1 + \delta\Psi_2 + \delta\Psi_3 \doteq 0 \quad \forall\, \delta\boldsymbol{y}\,. \tag{13}$$

In this contribution we extend CPD to transverse isotropy in a similar spirit as is common for CCM (see, e.g., Holzapfel et al., 2000; Spencer, 1984). To account for transverse isotropy in CCM, the stored energy function is extended by including additional invariants (for further details on invariants for isotropic functions of vectorial and tensorial arguments, see Adkins, 1960; Smith and Rivlin, 1957; Wang, 1970). These additional invariants are related to fibre stretch in the preferred direction. They depend on the transformation of an infinitesimal line element, i.e., by the action of the *tangent map* $\boldsymbol{F}$, and the direction of the fibres that characterises the anisotropy (the preferred direction). In this spirit, transverse isotropy is captured in CPD by invariants that are dependent on transformations of finite line and area elements, i.e., by the *secant maps* and the fibre direction. The subsequent sections detail the invariants necessary to capture transverse isotropy in CPD. The ensuing requirements on the potential energy for one-neighbour, two-neighbour and three-neighbour interactions are now discussed.

3.1. Potential energy for line elements

In PD the potential energy of the body is expressed as the integral of a non-local point-wise energy density over the body. For line elements (also known as bond-based interactions) this non-local energy density is defined as the potential energy double-density $\psi_1^{\shortmid}$ integrated over the horizon. The potential energy of the body due to one-neighbour interactions is thus given by

$$\Psi_1(\boldsymbol{y}) = \frac{1}{2!}\int_{\mathcal{B}_0}\int_{\mathcal{H}_0}\psi_1^{\shortmid}\,\mathrm{d}V^{\shortmid}\mathrm{d}V\,. \tag{14}$$

For *isotropic materials* restricted to only line element contributions, the potential energy double-density depends solely on the bond-based secant map, that is

$$\psi_1^{\shortmid} = \psi_1^{\shortmid}(\boldsymbol{\xi}^{\shortmid}) = \psi_1^{\shortmid}(\mathbb{F}^{\shortmid})\,. \tag{15}$$

Spatial objectivity is ensured if $\psi_1^{\shortmid}(\mathbb{F}^{\shortmid+}) = \psi_1^{\shortmid}(\mathbb{F}^{\shortmid})$ with $\mathbb{F}^{\shortmid+} = \boldsymbol{Q}\cdot\mathbb{F}^{\shortmid}$ for all proper orthogonal tensors $\boldsymbol{Q}\in\mathrm{SO}(3)$. Following in the spirit of CCM, we ensure spatial objectivity by letting

$$\psi_1^{\shortmid} = \psi_1^{\shortmid}(\mathbb{C}^{\shortmid}) \qquad \text{with} \qquad \mathbb{C}^{\shortmid} = \mathbb{F}^{\shortmid t}\cdot\mathbb{F}^{\shortmid} = \lambda^{\shortmid 2}\boldsymbol{E}^{\shortmid}\otimes\boldsymbol{E}^{\shortmid}\,, \tag{16}$$

as $\mathbb{C}^{\shortmid+} = [\boldsymbol{Q}\cdot\mathbb{F}^{\shortmid}]^t\cdot\boldsymbol{Q}\cdot\mathbb{F}^{\shortmid} = \mathbb{C}^{\shortmid}$, where $\mathbb{C}^{\shortmid}$ is a Cauchy–Green-type tensor. Furthermore, material objectivity of the double-density is ensured if $\psi_1^{\shortmid}(\mathbb{C}^{\shortmid}) = \psi_1^{\shortmid}(\boldsymbol{Q}\cdot\mathbb{C}^{\shortmid}\cdot\boldsymbol{Q}^t)$ for all proper orthogonal tensors $\boldsymbol{Q}\in\mathrm{SO}(3)$. Following the representation theorem for tensor functions (Zheng, 1994), the scalar-valued tensor function $\psi_1^{\shortmid}(\mathbb{C}^{\shortmid})$ may be expressed in terms of the principal invariants of $\mathbb{C}^{\shortmid}$. Possible invariants of $\mathbb{C}^{\shortmid}$ are, for example, $\mathrm{inv}_{\mathbb{C}^{\shortmid}} = \mathrm{Tr}\{\mathbb{C}^{\shortmid}, \mathbb{C}^{\shortmid 2}, \mathbb{C}^{\shortmid 3}\} = \{\lambda^{\shortmid 2}, \lambda^{\shortmid 4}, \lambda^{\shortmid 6}\}$, i.e., the even powers of the bond stretch. The potential energy double-density for *isotropic materials* can therefore be *sufficiently* expressed using a single invariant as

$$\psi_1^{\shortmid} = \psi_1^{\shortmid}(I_1) \qquad \text{with} \qquad I_1 := \lambda^{\shortmid 2}\,. \tag{17}$$

For *anisotropic materials*, the deformation of the material with a single preferred direction also depends on the

fibre orientation. The direction of a fibre at point $\boldsymbol{X}$ in $\mathcal{B}_0$ is denoted by $\boldsymbol{A} = \boldsymbol{A}(\boldsymbol{X})$, $|\boldsymbol{A}| = 1$, as shown in Figure 2(a). It is convenient to introduce the direction cosine $\alpha^{\shortmid} = \alpha^{\shortmid}(\boldsymbol{X}^{\shortmid}; \boldsymbol{X})$ as a measure of the relative direction of $\boldsymbol{\Xi}^{\shortmid}$ with respect to $\boldsymbol{A}$:

$$\alpha^{\shortmid} := \boldsymbol{A} \cdot \boldsymbol{E}^{\shortmid} = |A|\,|E^{\shortmid}| \cos\theta^{\shortmid} = \cos\theta^{\shortmid} \qquad \text{with} \qquad \operatorname{sign}(\alpha^{\shortmid}) = \pm 1 \qquad \text{and} \qquad \alpha^{\shortmid}_{\oplus} := |\,\alpha^{\shortmid}\,| \,. \tag{18}$$

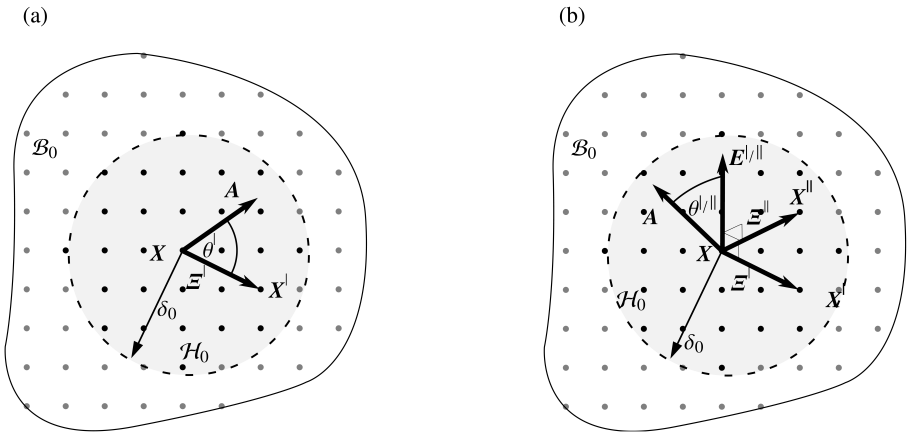

Figure 2: Point-wise fibre direction $\boldsymbol{A}$ and associated kinematic measures for (a) line elements and (b) area elements

To introduce physically motivated directional agnosticism, the line element energy double-density for transverse isotropy is prescribed to be a function of the Cauchy–Green-like strain tensor $\mathbb{C}^{\shortmid}$ and the structural tensor $\mathbb{A}$, i.e.,

$$\psi^{\shortmid}_1 = \psi^{\shortmid}_1(\mathbb{C}^{\shortmid}, \mathbb{A}) \qquad \text{with} \qquad \mathbb{A} := \boldsymbol{A} \otimes \boldsymbol{A} \,. \tag{19}$$

If the anisotropy results solely from the presence of fibres, the energy remains unchanged if the deformation and the fibres undergo the same rigid rotation superposed upon the material configuration, a situation denoted here as material objectivity. The potential energy double-density is an objective function of $\mathbb{C}^{\shortmid}$ and $\mathbb{A}$ if the condition

$$\psi^{\shortmid}_1(\mathbb{C}^{\shortmid}, \mathbb{A}) \stackrel{!}{=} \psi^{\shortmid}_1(\boldsymbol{Q} \cdot \mathbb{C}^{\shortmid} \cdot \boldsymbol{Q}^{\mathrm{T}}, \boldsymbol{Q} \cdot \mathbb{A} \cdot \boldsymbol{Q}^{\mathrm{T}}) \,, \tag{20}$$

holds for all proper orthogonal tensors $\boldsymbol{Q} \in \mathrm{SO}(3)$. The potential energy double-density in Eq. (19) can be written in terms of the invariants associated with $\mathbb{C}^{\shortmid}$, the invariants associated with $\mathbb{A}$, and the invariants associated with the combination of the tensors, i.e.,

$$\psi^{\shortmid}_1 = \psi^{\shortmid}_1(\mathrm{Tr}\{\mathbb{C}^{\shortmid},\, \mathbb{C}^{\shortmid 2},\, \mathbb{C}^{\shortmid 3},\, \mathbb{A},\, \mathbb{A}^2,\, \mathbb{A}^3,\, \mathbb{C}^{\shortmid} \cdot \mathbb{A},\, \mathbb{C}^{\shortmid} \cdot \mathbb{A}^2,\, \mathbb{C}^2 \cdot \mathbb{A},\, \mathbb{C}^{\shortmid 2} \cdot \mathbb{A}^2\}) \,, \tag{21}$$

where the invariants are given by

$$\begin{aligned}
\mathrm{inv}_{\mathbb{C}^{\shortmid}} &= \mathrm{Tr}\{\mathbb{C}^{\shortmid},\, \mathbb{C}^{\shortmid 2},\, \mathbb{C}^{\shortmid 3}\} = \{\lambda^{\shortmid 2},\, \lambda^{\shortmid 4},\, \lambda^{\shortmid 6}\} \,, \\
\mathrm{inv}_{\mathbb{A}} &= \mathrm{Tr}\{\mathbb{A},\, \mathbb{A}^2,\, \mathbb{A}^3\} = \{1,\, 1,\, 1\} \,, \\
\mathrm{inv}_{\mathbb{C}^{\shortmid},\mathbb{A}} &= \mathrm{Tr}\{\mathbb{C}^{\shortmid} \cdot \mathbb{A},\, \mathbb{C}^{\shortmid} \cdot \mathbb{A}^2,\, \mathbb{C}^{\shortmid 2} \cdot \mathbb{A},\, \mathbb{C}^{\shortmid 2} \cdot \mathbb{A}^2\} = \{\lambda^{\shortmid 2}\alpha^{\shortmid 2},\, [\lambda^{\shortmid 2}\alpha^{\shortmid 2}]^2,\, \lambda^{\shortmid 4}\alpha^{\shortmid 2},\, [\lambda^{\shortmid 4}\alpha^{\shortmid 2}]^2\} \,.
\end{aligned} \tag{22}$$

Thus, the energy double-density can be *sufficiently* expressed as

$$\begin{aligned}\psi_1^{\shortmid} &= \psi_1^{\shortmid}(\,\mathrm{Tr}\{\mathbb{C}^{\shortmid},\, \mathbb{C}^{\shortmid}\cdot\mathbb{A},\, \mathbb{C}^{\shortmid 2}\cdot\mathbb{A}\}\,)\\ &= \psi_1^{\shortmid}(I_1, I_4, I_5) \qquad \text{with} \qquad \mathrm{I}_1 = \lambda^{\shortmid 2} \quad , \quad \mathrm{I}_4 = \alpha^{\shortmid 2}\lambda^{\shortmid 2} \quad , \quad \mathrm{I}_5 = \alpha^{\shortmid 2}\lambda^{\shortmid 4}\,. \end{aligned} \tag{23}$$

Here I_1 refers to the invariant associated with the isotropic part of the line element contribution. The invariants associated with the preferred direction for line element contributions are I_4 and I_5. We intentionally reserve I_2 and I_3 for the invariants associated with isotropic area elements and volume elements that will be defined in Sections 3.2 and 3.3, respectively. Finally, the line element potential energy double-density for transverse isotropy that satisfies material objectivity can equivalently be expressed in the following reduced format

$$\psi_1^{\shortmid}(\lambda^{\shortmid 2},\, \alpha^{\shortmid 2}\lambda^{\shortmid 2},\, \alpha^{\shortmid 2}\lambda^{\shortmid 4}) = \psi_1^{\shortmid}(\lambda^{\shortmid 2},\, \alpha^{\shortmid 2}) \qquad \Rightarrow \qquad \psi_1^{\shortmid} \equiv \psi_1^{\shortmid *}(\lambda^{\shortmid},\, \alpha_{\oplus}^{\shortmid})\,. \tag{24}$$

Note that the stretch $\lambda^{\shortmid}$ is always a positive value by definition and therefore, unlike $\alpha_{\oplus}^{\shortmid}$ (see Eq. 18), using a notation such as $\lambda_{\oplus}^{\shortmid}$ would be superfluous.

3.2. Potential energy for area elements

The potential energy associated with area elements Ψ_2 is given as the integral of a non-local point-wise energy density over the body. For area elements, this is defined as the potential energy triple-density $\psi_2{}^{\shortmid/\shortparallel}$ integrated over the horizon twice. Thus Ψ_2 is given by

$$\Psi_2\,(\mathbf{y}) = \frac{1}{3!}\int_{\mathcal{B}_0}\int_{\mathcal{H}_0}\int_{\mathcal{H}_0} \psi_2^{\shortmid/\shortparallel}\,\mathrm{d}V^{\shortparallel}\mathrm{d}V^{\shortmid}\mathrm{d}V\,. \tag{25}$$

The potential energy triple-density for *isotropic materials* depends on the double-bond based co-secant map, that is

$$\psi_2^{\shortmid/\shortparallel} = \psi_2^{\shortmid/\shortparallel}(\boldsymbol{\xi}^{\shortmid/\shortparallel}) = \psi_2^{\shortmid/\shortparallel}(\mathbb{F}^{\shortmid/\shortparallel})\,. \tag{26}$$

To ensure the spatial objectivity, i.e., $\psi_2^{\shortmid/\shortparallel}(\mathbb{F}^{\shortmid/\shortparallel +}) = \psi_2^{\shortmid/\shortparallel}(\mathbb{F}^{\shortmid/\shortparallel})$ with $\mathbb{F}^{\shortmid/\shortparallel +} = \boldsymbol{Q}\cdot\mathbb{F}^{\shortmid/\shortparallel}$ for all proper orthogonal tensors $\boldsymbol{Q}\in\mathrm{SO}(3)$, we require

$$\psi_2^{\shortmid/\shortparallel} = \psi_2^{\shortmid/\shortparallel}(\mathbb{C}^{\shortmid/\shortparallel}) \qquad \text{with} \qquad \mathbb{C}^{\shortmid/\shortparallel} = \mathbb{F}^{\shortmid/\shortparallel t}\cdot\mathbb{F}^{\shortmid/\shortparallel} = \lambda^{\shortmid/\shortparallel 2}\boldsymbol{E}^{\shortmid/\shortparallel}\otimes\boldsymbol{E}^{\shortmid/\shortparallel}\,, \tag{27}$$

where $\mathbb{C}^{\shortmid/\shortparallel}$ is a Cauchy–Green-type tensor. Material objectivity of the triple-density is ensured if $\psi_2^{\shortmid/\shortparallel}(\mathbb{C}^{\shortmid/\shortparallel}) = \psi_2^{\shortmid/\shortparallel}(\boldsymbol{Q}\cdot\mathbb{C}^{\shortmid/\shortparallel}\cdot\boldsymbol{Q}^t)$ for all proper orthogonal tensors $\boldsymbol{Q}\in\mathrm{SO}(3)$. If $\psi_2^{\shortmid/\shortparallel}(\mathbb{C}^{\shortmid/\shortparallel})$ is an invariant of the symmetric tensor $\mathbb{C}^{\shortmid/\shortparallel}$ it may be expressed in terms of the principal invariants of $\mathbb{C}^{\shortmid/\shortparallel}$. Possible invariants of $\mathbb{C}^{\shortmid/\shortparallel}$ are, for example,

$$\mathrm{inv}_{\mathbb{C}^{\shortmid/\shortparallel}} = \{\mathrm{Tr}\,\mathbb{C}^{\shortmid/\shortparallel} = [\lambda^{\shortmid/\shortparallel}]^2,\, \mathrm{Tr}\,[\mathbb{C}^{\shortmid/\shortparallel}]^2 = [\lambda^{\shortmid/\shortparallel}]^4,\, \mathrm{Tr}\,[\mathbb{C}^{\shortmid/\shortparallel}]^3 = [\lambda^{\shortmid/\shortparallel}]^6\}\,, \tag{28}$$

i.e., the even powers of the double-bond stretch. The potential energy triple-density for isotropic materials can therefore be expressed as a function of a single invariant by

$$\psi_2^{\shortmid/\shortparallel} = \psi_2^{\shortmid/\shortparallel}(I_2) \quad \text{with} \quad I_2 = [\lambda^{\shortmid/\shortparallel}]^2\,. \tag{29}$$

The direction cosine $\alpha^{\shortmid/\shortparallel} = \alpha^{\shortmid/\shortparallel}(\boldsymbol{X}^{\shortmid}, \boldsymbol{X}^{\shortparallel}; \boldsymbol{X})$, as indicated in Figure 2(b), captures the direction of the normal of the

plane formed by a point and two of its neighbours in the two-neighbour set, i.e., $\boldsymbol{E}^{|_{\prime}|\!|}$, with respect to $\boldsymbol{A}$, that is

$$\alpha^{|_{\prime}|\!|} = \boldsymbol{A}\cdot\boldsymbol{E}^{|_{\prime}|\!|} = |A||E^{|_{\prime}|\!|}|\cos\theta^{|_{\prime}|\!|} = \cos\theta^{|_{\prime}|\!|} \qquad \text{with} \qquad \operatorname{sign}(\alpha^{|_{\prime}|\!|}) = \pm 1 \qquad \text{and} \qquad \alpha_{\oplus}^{|_{\prime}|\!|} = |\alpha^{|_{\prime}|\!|}|\,. \tag{30}$$

Physically, $\alpha^{|_{\prime}|\!|}$ describes the orientation of the normal vector $\boldsymbol{E}^{|_{\prime}|\!|}$ with respect to the fibre direction $\boldsymbol{A}$; see Figure 3. In particular if the direction of a fibre at point $\boldsymbol{X}$ is tangential to the plane spanned by $\boldsymbol{\Xi}^{|}$ and $\boldsymbol{\Xi}^{\|}$, then for that set of neighbours $\alpha^{|_{\prime}|\!|} = 0$. Conversely, if the direction of a fibre is orthogonal to $\boldsymbol{\Xi}^{|}$ and $\boldsymbol{\Xi}^{\|}$, then $\alpha^{|_{\prime}|\!|} = 1$, i.e., $\alpha^{|_{\prime}|\!|}$ assumes its maximum value.

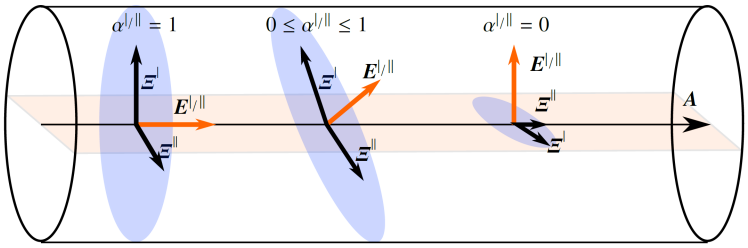

Figure 3: Planes formed by a point and two neighbours. A plane perpendicular to the fibre direction (left), randomly oriented (middle) and parallel to the fibre orientation (right) have different values of $\alpha^{|_{\prime}|\!|}$.

As for the line element contributions, physically motivated directional agnosticism is ensured by stipulating that the area element potential energy triple-density for transverse isotropy depends on $\mathbb{C}^{|_{\prime}|\!|}$ and the structural tensor $\mathbb{A}$, i.e.,

$$\psi_2^{|_{\prime}|\!|} = \psi_2^{|_{\prime}|\!|}(\mathbb{C}^{|_{\prime}|\!|}, \mathbb{A}). \tag{31}$$

Assuming the anisotropy only results from fibres, the potential energy triple-density is a materially objective function of $\mathbb{C}^{|_{\prime}|\!|}$ and $\mathbb{A}$ if the condition

$$\psi_2^{|_{\prime}|\!|}(\mathbb{C}^{|_{\prime}|\!|}, \mathbb{A}) \overset{!}{=} \psi_2^{|_{\prime}|\!|}(\boldsymbol{Q}\cdot\mathbb{C}^{|_{\prime}|\!|}\cdot\boldsymbol{Q}^{\mathrm{T}}, \boldsymbol{Q}\cdot\mathbb{A}\cdot\boldsymbol{Q}^{\mathrm{T}}) \tag{32}$$

holds for all proper orthogonal tensors $\boldsymbol{Q} \in \mathrm{SO}(3)$. The interaction triple-density in Eq. (31) can be written in terms of the invariants associated with $\mathbb{C}^{|_{\prime}|\!|}$, the invariants associated with $\mathbb{A}$, and the invariants associated with the combination of these tensors, i.e.,

$$\psi_2^{|_{\prime}|\!|} = \psi_2^{|_{\prime}|\!|}(\mathrm{Tr}\{\mathbb{C}^{|_{\prime}|\!|}, [\mathbb{C}^{|_{\prime}|\!|}]^2, [\mathbb{C}^{|_{\prime}|\!|}]^3, \mathbb{A}, \mathbb{A}^2, \mathbb{A}^3, \mathbb{C}^{|_{\prime}|\!|}\cdot\mathbb{A}, \mathbb{C}^{|_{\prime}|\!|}\cdot\mathbb{A}^2, [\mathbb{C}^{|_{\prime}|\!|}]^2\cdot\mathbb{A}, [\mathbb{C}^{|_{\prime}|\!|}]^2\cdot\mathbb{A}^2\})\,. \tag{33}$$

These invariants can be expressed as follows:

$$\begin{aligned}
\mathrm{inv}_{\mathbb{C}^{|_{\prime}|\!|}} &= \mathrm{Tr}\{\mathbb{C}^{|_{\prime}|\!|}, [\mathbb{C}^{|_{\prime}|\!|}]^2, [\mathbb{C}^{|_{\prime}|\!|}]^3\} = \{[\lambda^{|_{\prime}|\!|}]^2, [\lambda^{|_{\prime}|\!|}]^4, [\lambda^{|_{\prime}|\!|}]^6\}\,,\\
\mathrm{inv}_{\mathbb{A}} &= \mathrm{Tr}\{\mathbb{A}, \mathbb{A}^2, \mathbb{A}^3\} = \{1, 1, 1\}\,,\\
\mathrm{inv}_{\mathbb{C}^{|_{\prime}|\!|},\mathbb{A}} &= \mathrm{Tr}\{\mathbb{C}^{|_{\prime}|\!|}\cdot\mathbb{A}, \mathbb{C}^{|_{\prime}|\!|}\cdot\mathbb{A}^2, [\mathbb{C}^{|_{\prime}|\!|}]^2\cdot\mathbb{A}, [\mathbb{C}^{|_{\prime}|\!|}]^2\cdot\mathbb{A}^2\}\\
&= \{[\lambda^{|_{\prime}|\!|}]^2[\alpha^{|_{\prime}|\!|}]^2, [[\lambda^{|_{\prime}|\!|}]^2[\alpha^{|_{\prime}|\!|}]^2]^2, [\lambda^{|_{\prime}|\!|}]^4[\alpha^{|_{\prime}|\!|}]^2, [[\lambda^{|_{\prime}|\!|}]^4[\alpha^{|_{\prime}|\!|}]^2]^2\}\,.
\end{aligned}$$

This allows the energy triple-density to be *sufficiently* characterised as

$$\psi_2^{|/\|} = \psi_2^{|/\|}(\,\mathrm{Tr}\{\mathbb{C}^{|/\|},\ \mathbb{C}^{|/\|}\cdot\mathbb{A},\ [\mathbb{C}^{|/\|}]^2\cdot\mathbb{A}\}\,) \tag{34}$$

$$= \psi_2^{|/\|}(I_2, I_6, I_7) \qquad \text{with} \qquad I_2 = [\lambda^{|/\|}]^2 \quad , \quad I_6 = [\alpha^{|/\|}]^2[\lambda^{|/\|}]^2 \quad , \quad I_7 = [\alpha^{|/\|}]^2[\lambda^{|/\|}]^4\,. \tag{35}$$

Thus the final equivalent expression for the potential energy triple-density for area elements is

$$\psi_2^{|/\|}([\lambda^{|/\|}]^2, [\alpha^{|/\|}]^2[\lambda^{|/\|}]^2, [\alpha^{|/\|}]^2[\lambda^{|/\|}]^4) = \psi_2^{|/\|}([\lambda^{|/\|}]^2, [\alpha^{|/\|}]^2) \qquad \Rightarrow \qquad \psi_2^{|/\|} \equiv \psi_2^{|/\|*}(\lambda^{|/\|}, \alpha_\oplus^{|/\|})\,. \tag{36}$$

Again, since the area stretch $\lambda^{|/\|}$ is inherently positive, unlike $\alpha_\oplus^{|/\|}$, using a notation such as $\lambda_\oplus^{|/\|}$ would be superfluous.

Remark 3. For problems in two dimensions, $\boldsymbol{E}^{|/\|}$ is out of the plane, and as $\boldsymbol{A}$ is in the plane, $\alpha^{|/\|} = 0$. It follows from a physical perspective that the inclusion of transverse isotropy for two-neighbour interactions does not make sense in two dimensions. The conclusion is that contributions to the potential energy density for transverse isotropy in two-dimensional problems stems solely from one-neighbour interactions. □

3.3. Potential energy for volume elements

The potential energy of the body associated with volume elements Ψ_3 is given as the integral of a non-local pointwise energy density over the body. For volume elements this is defined as the potential energy quadruple-density ${\psi_3}^{|/\|/\|\|}$ integrated over the horizon thrice. The potential energy Ψ_3 is thus given by

$$\Psi_3\,(\mathbf{y}) = \frac{1}{4!}\int_{\mathcal{B}_0}\int_{\mathcal{H}_0}\int_{\mathcal{H}_0}\int_{\mathcal{H}_0} \psi_3^{|/\|/\|\|}\mathrm{d}V^{\|}\mathrm{d}V^{|}\mathrm{d}V\,. \tag{37}$$

For isotropic materials where the energy of volume elements is also included, the energy depends on the triple-bond volume measure map $\psi_3^{|/\|/\|\|} = \psi_3^{|/\|/\|\|}(\boldsymbol{\xi}^{|/\|/\|\|}) = \psi_3^{|/\|/\|\|}(\mathbb{F}^{|/\|/\|\|}) = \psi_3^{|/\|/\|\|}(\mathbb{C}^{|/\|/\|\|}) = \psi_3^{|/\|/\|\|}([\lambda^{|/\|/\|\|}]^3)$. As $\xi^{|/\|/\|\|}$, $\mathbb{F}^{|/\|/\|\|}$ and $\mathbb{C}^{|/\|/\|\|}$ are all scalars, the potential energy quadruple-density for isotropic materials can be expressed by a single invariant

$$\psi_3^{|/\|/\|\|} = \psi_3^{|/\|}(I_3) \quad \text{with} \quad I_3 = \lambda^{|/\|/\|\|}\,. \tag{38}$$

Remark 4. As the triple-bond based material measure map is a scalar ratio indicating volume change of a finite element, it is not possible to define a direction cosine $\alpha^{|/\|/\|\|}$ between this map and the fibre direction $\boldsymbol{A}$. Therefore, the triple-bond potential energy cannot be extended to include anisotropy. □

3.4. Additive decomposition of potential energy densities

The potential energy densities for materials where the response of the material and the fibre to external loading differs can be expressed additively as

$$\psi_1^{|} = \psi_{1,\mathrm{iso}}^{|}(I_1) + \psi_{1,\mathrm{ani}}^{|}(I_4, I_5) \qquad \text{and} \qquad \psi_2^{|/\|} = \psi_{2,\mathrm{iso}}^{|/\|}(I_2) + \psi_{2,\mathrm{ani}}^{|/\|}(I_6, I_7)\,. \tag{39}$$

4. Governing equations

Recall that equilibrium is obtained by finding the stationary point of the energy functional with respect to all admissible variations (Eq. 13). This procedure is now utilised to realise the contribution to the governing equations

associated with line-, area- and volume elements, along with the expressions for the respective interaction forces. For a more detailed derivation, see Javili et al. (2019a, 2021b).

4.1. Contributions to variations of potential energy

The variation of the potential energy $\delta\Psi$ consists of the sum $\delta\Psi_1 + \delta\Psi_2 + \delta\Psi_3$ due to the contributions from one-neighbour, two-neighbour, and three-neighbour interactions, corresponding to line, area and volume elements, respectively. The individual contributions are now briefly discussed in Sections 4.1.1, 4.1.2 and 4.1.3. In what follows, it is assumed that the field $\boldsymbol{y}$ and its variation $\delta\boldsymbol{y}$ are integrable, $\boldsymbol{y}$ satisfies the prescribed displacements, and $\delta\boldsymbol{y} = \boldsymbol{0}$ where the displacements are prescribed. That is, we assume the fields to be admissible.

4.1.1. Contribution from line elements

The contribution to the governing equation from Ψ_1 in Eq. (14) is found by applying the chain rule and the definition of the relative deformation map $\boldsymbol{\xi}^{\shortmid}$ in Eq. $(2)_2$ as

$$\delta\Psi_1(\boldsymbol{y}) = \frac{1}{2!}\int_{\mathcal{B}_0}\int_{\mathcal{H}_0} \partial_{\lambda^{\shortmid}}\psi_1^{\shortmid}\,\boldsymbol{e}^{\shortmid}\cdot\delta\boldsymbol{\xi}^{\shortmid}\,\mathrm{d}V^{\shortmid}\,\mathrm{d}V\,, \tag{40}$$

which after some mathematical steps yields

$$\delta\Psi_1(\boldsymbol{y}) = -\int_{\mathcal{B}_0}\int_{\mathcal{H}_0} \boldsymbol{p}^{\shortmid}\,\mathrm{d}V^{\shortmid}\cdot\delta\boldsymbol{y}\,\mathrm{d}V\,. \tag{41}$$

Here

$$\boldsymbol{p}^{\shortmid}(\boldsymbol{X}) := \partial_{\lambda^{\shortmid}}\psi_1^{\shortmid}\,\boldsymbol{e}^{\shortmid} + \cancelto{\boldsymbol{0}}{\partial_{\alpha^{\shortmid}}\psi_1^{\shortmid}\,\partial_{\xi^{\shortmid}}\alpha^{\shortmid}} = \partial_{\lambda^{\shortmid}}\psi_1^{\shortmid}\boldsymbol{e}^{\shortmid} \qquad \text{with} \qquad [\boldsymbol{p}^{\shortmid}] = \text{force/m}^6 \tag{42}$$

denotes the bond-wise interaction force double-density with its integral over $\mathcal{H}_0$ rendering a point-wise force density with units force/m^3. For more details on the derivation of the governing equations for one-neighbour interactions, see Steinmann et al. (2023).

4.1.2. Contribution from area elements

Similarly, the stationary point and contribution to the governing equations from Ψ_2 in Eq. (25) are obtained using the chain rule, Eq. $(4)_2$ and the property $\delta\boldsymbol{\xi}^{\shortmid/\shortmid\shortmid} = \delta\boldsymbol{\xi}^{\shortmid}\times\boldsymbol{\xi}^{\shortmid\shortmid} + \boldsymbol{\xi}^{\shortmid}\times\delta\boldsymbol{\xi}^{\shortmid\shortmid}$, yielding

$$\delta\,\Psi_2(\boldsymbol{y}) = \frac{1}{3!}\int_{\mathcal{B}_0}\int_{\mathcal{H}_0}\int_{\mathcal{H}_0} \partial_{\lambda^{\shortmid/\shortmid\shortmid}}\psi_2^{\shortmid/\shortmid\shortmid}\,\boldsymbol{e}^{\shortmid/\shortmid\shortmid}\cdot\delta\,\boldsymbol{\xi}^{\shortmid/\shortmid\shortmid}\,\mathrm{d}V^{\shortmid\shortmid}\mathrm{d}V^{\shortmid}\mathrm{d}V\,, \tag{43}$$

that after some mathematical steps reads

$$\delta\,\Psi_2(\boldsymbol{y}) = -\int_{\mathcal{B}_0}\int_{\mathcal{H}_0}\int_{\mathcal{H}_0} \boldsymbol{p}^{\shortmid/\shortmid\shortmid}\,\mathrm{d}V^{\shortmid\shortmid}\mathrm{d}V^{\shortmid}\cdot\delta\,\boldsymbol{y}\,\mathrm{d}V\,. \tag{44}$$

The interaction force triple-density for two-neighbour interactions is given by

$$\boldsymbol{p}^{\shortmid/\shortmid\shortmid}(\boldsymbol{X}) := \boldsymbol{\xi}^{\shortmid\shortmid}\times[\partial_{\lambda^{\shortmid/\shortmid\shortmid}}\psi_2^{\shortmid/\shortmid\shortmid}\,\boldsymbol{e}^{\shortmid/\shortmid\shortmid} + \cancelto{\boldsymbol{0}}{\partial_{\alpha^{\shortmid/\shortmid\shortmid}}\psi_2^{\shortmid/\shortmid\shortmid}\,\partial_{\xi^{\shortmid/\shortmid\shortmid}}\alpha^{\shortmid/\shortmid\shortmid}}] = \boldsymbol{\xi}^{\shortmid\shortmid}\times\partial_{\lambda^{\shortmid/\shortmid\shortmid}}\psi_2^{\shortmid/\shortmid\shortmid}\,\boldsymbol{e}^{\shortmid/\shortmid\shortmid} \qquad \text{with} \qquad [\boldsymbol{p}^{\shortmid/\shortmid\shortmid}] = \text{force/m}^9\,. \tag{45}$$

Integrating the area element interaction force triple-density twice over $\mathcal{H}_0$ renders a point-wise force density with units force/m^3. For more details on the derivation of the governing equations and force density for area elements, see Laurien et al. (2024).

4.1.3. Contribution from volume elements

The stationary point and contribution to the governing equation from Ψ_3 in Eq. (37) follows as

$$\delta\,\Psi_3(\boldsymbol{y}) = \frac{1}{4!}\int_{\mathcal{B}_0}\int_{\mathcal{H}_0}\int_{\mathcal{H}_0}\int_{\mathcal{H}_0} \partial_{\lambda^{\mathrm{I}/\mathrm{II}/\mathrm{III}}}\psi_3{}^{\mathrm{I}/\mathrm{II}/\mathrm{III}}\boldsymbol{e}^{\mathrm{I}/\mathrm{II}/\mathrm{III}}\cdot\delta\boldsymbol{\xi}^{\mathrm{I}/\mathrm{II}/\mathrm{III}}\,\mathrm{d}V^{\mathrm{III}}\,\mathrm{d}V^{\mathrm{II}}\,\mathrm{d}V^{\mathrm{I}}\,, \tag{46}$$

which after some mathematical steps can be expressed as

$$\delta\,\Psi_3(\boldsymbol{y}) = -\int_{\mathcal{B}_0}\int_{\mathcal{H}_0}\int_{\mathcal{H}_0}\int_{\mathcal{H}_0} \boldsymbol{p}^{\mathrm{I}/\mathrm{II}/\mathrm{III}}\,\mathrm{d}V^{\mathrm{III}}\,\mathrm{d}V^{\mathrm{II}}\mathrm{d}V^{\mathrm{I}}\cdot\delta\,\boldsymbol{y}\,\mathrm{d}V\,. \tag{47}$$

The interaction force quadruple-density for three-neighbour interactions is defined by

$$\boldsymbol{p}^{\mathrm{I}/\mathrm{II}/\mathrm{III}}(\boldsymbol{X}) := \left[\boldsymbol{\xi}^{\mathrm{II}}\times\boldsymbol{\xi}^{\mathrm{III}}\right]\,\partial_{\lambda^{\mathrm{I}/\mathrm{II}/\mathrm{III}}}\psi_3{}^{\mathrm{I}/\mathrm{II}/\mathrm{III}}\,\boldsymbol{e}^{\mathrm{I}/\mathrm{II}/\mathrm{III}} \qquad \text{with} \qquad [\boldsymbol{p}^{\mathrm{I}/\mathrm{II}/\mathrm{III}}] = \mathrm{force}/\mathrm{m}^{12}\,. \tag{48}$$

Integrating the volume element interaction force quadruple-density thrice over $\mathcal{H}_0$ renders a point-wise force density with units force/m^3. See Laurien et al. (2024) for further information.

4.2. Balance of linear momentum

The balance of linear momentum for quasi-static motion, neglecting external forces, is obtained by substituting Eqs (41), $(44)_2$ and $(46)_2$ into Eq. (13), yielding

$$-\int_{\mathcal{H}_0}\boldsymbol{p}^{\mathrm{I}}\mathrm{d}V^{\mathrm{I}} - \int_{\mathcal{H}_0}\int_{\mathcal{H}_0}\boldsymbol{p}^{\mathrm{I}/\mathrm{II}}\,\mathrm{d}V^{\mathrm{II}}\mathrm{d}V^{\mathrm{I}} - \int_{\mathcal{H}_0}\int_{\mathcal{H}_0}\int_{\mathcal{H}_0}\boldsymbol{p}^{\mathrm{I}/\mathrm{II}/\mathrm{III}}\,\mathrm{d}V^{\mathrm{III}}\mathrm{d}V^{\mathrm{II}}\mathrm{d}V^{\mathrm{I}} = \boldsymbol{0}\,. \tag{49}$$

4.3. Balance of angular momentum

Following Javili et al. (2019a), the balance of angular momentum is obtained from the global moment balance and subsequent application of the linear momentum equation which gives

$$\int_{\mathcal{H}_0}\boldsymbol{\xi}^{\mathrm{I}}\times\boldsymbol{p}^{\mathrm{I}}\mathrm{d}V^{\mathrm{I}} + \int_{\mathcal{H}_0}\int_{\mathcal{H}_0}\boldsymbol{\xi}^{\mathrm{I}}\times\boldsymbol{p}^{\mathrm{I}/\mathrm{II}}\,\mathrm{d}V^{\mathrm{II}}\mathrm{d}V^{\mathrm{I}} - \int_{\mathcal{H}_0}\int_{\mathcal{H}_0}\int_{\mathcal{H}_0}\boldsymbol{\xi}^{\mathrm{I}}\times\boldsymbol{p}^{\mathrm{I}/\mathrm{II}/\mathrm{III}}\,\mathrm{d}V^{\mathrm{III}}\mathrm{d}V^{\mathrm{II}}\mathrm{d}V^{\mathrm{I}} \doteq \boldsymbol{0}\,. \tag{50}$$

This condition is sufficiently met when ψ_1^{I}, $\psi_2^{\mathrm{I}/\mathrm{II}}$ and $\psi_3^{\mathrm{I}/\mathrm{II}/\mathrm{III}}$ are expressed in terms of the scalar invariants described in Eqs (24), (36) and (38). The resulting interaction force densities $\boldsymbol{p}^{\mathrm{I}}$, $\boldsymbol{p}^{\mathrm{I}/\mathrm{II}}$, $\boldsymbol{p}^{\mathrm{I}/\mathrm{II}/\mathrm{III}}$ in Eqs (42), (45), and (48) are parallel to $\boldsymbol{\xi}^{\mathrm{I}}$ and therefore satisfy Eq. (50).

5. Computational Aspects

The numerical implementation is performed in the Julia programming language (Bezanson et al., 2017) and builds on the framework introduced in Javili et al. (2020). For the sake of transparancy and brevity, the algorithm for a problem consisting only of line and area elements is shown in the flowchart presented in Figure 4. The corresponding algorithm that includes volume elements is analogous and thus omitted here.

In the pre-processing stage, the necessary data structures are created and populated. The direction cosines $\alpha^{|}_{\oplus}$ and $\alpha^{|||}_{\oplus}$, as well as the density functions $\rho(\alpha^{|}_{\oplus})$ and $\rho(\alpha^{|||}_{\oplus})$, introduced in Section 6, for each neighbour of each grid point are then calculated.

A Newton-Raphson solution scheme is used to solve the non-linear system of discrete equations. Automatic differentiation using hyper–dual numbers is employed to calculate the contributions to the residual ($\mathbb{R}$), and tangent ($\mathbb{K}$) following Firooz et al. (2024).

In the post-processing stage, effective point-wise quantities $\boldsymbol{F}$, $\boldsymbol{P}$ and $\boldsymbol{a}$ (see Eqs. (60), $(61)_b$) are calculated.

6. Forms of the potential energy densities for transverse isotropy

The general requirements for the various isotropic and anisotropic energy density contributions are now outlined. Thereafter a series of examples based solely on line element interactions is presented to demonstrate the ability to recover various transverse isotropy formulations found in the literature using the general format of Eq. (24). Further examples are given to illustrate the versatility of the model when extended to include area and volume elements to accommodate materials that exhibit varying Poisson's effect and to simulate three-dimensional bodies with more than one preferred direction. Finally, a comparison between the line element (Eq. 24) and area element formulations (Eq. 36) motivates the introduction of the novel area element formulation.

6.1. Solely line element interactions

A harmonic isotropic potential energy double-density is commonly used for line element interactions (or bond-based peridynamics), see for example (Javili et al., 2020). This takes the form

$$\psi^{|}_{1,\text{iso}}(\lambda^{|}) = \frac{1}{2}\, C_{1,\text{iso}}\, \Xi^{|}\, [\lambda^{|} - 1]^2\,, \tag{51}$$

where $C_{1,\text{iso}}$ is the bond stiffness coefficient. The analogous general format for the transversely isotropic potential energy double-density, that also ensures the material configuration is in equilibrium (or "stress-free") for zero deformation, is given by

$$\psi^{|}_{1,\text{ani}}(\lambda^{|}, \alpha^{|}_{\oplus}) = \frac{1}{2}\, C_{1,\text{ani}}\, \rho(\alpha^{|}_{\oplus})\, \Xi^{|}\, [\lambda^{|} - 1]^2\,. \tag{52}$$

Here the bond stiffness coefficient $C_{1,\text{ani}}$ multiplies a weighting function ρ of the relative direction of the bond $\alpha^{|}_{\oplus}$. Using Eq. (18), $\alpha^{|}_{\oplus}$ is obtained from the preferred direction $\boldsymbol{A}$ or equivalently from the orientation angle γ, where γ is defined anticlockwise from the horizontal. Various choices for the density function ρ are now discussed.

6.1.1. ρ as a scaling function

Several models for transverse isotropy in PD include a function which scales the bond stiffness coefficient $C_{1,\text{ani}}$ based on its relative direction (Ghajari et al., 2014; Hu et al., 2012; Tian and Zhou, 2021).

Figure 5 shows the deformation of an initially unit square with a preferred fibre direction $\gamma = 45°$. The unit square is subjected to 100% uniaxial extension enforced by prescribing a linear variation of the displacements within a region of thickness δ. The domain is discretised using 41×41 grid points with a horizon-to-grid spacing ratio of $\delta/\Delta = 3$.

The influence of the choice of $\rho(\alpha^{|}_{\oplus})$ on the response is now detailed. The different options proposed are normalised such that

$$\int_{\mathcal{H}_0} \rho(\alpha^{|}_{\oplus})\, \mathrm{d}V^{|} = 1\,. \tag{53}$$

That is, the combined stiffness of the neighbourhood remains unchanged, but the distribution of the stiffness differs based on the choice of $\rho(\alpha^{|}_{\oplus})$. The polar plots of $\rho(\alpha^{|}_{\oplus})$ displayed in Figure 5 show the normalised value of $\rho(\alpha^{|}_{\oplus})$ such that $\rho(\alpha^{|}_{\oplus})_{\max} = 1$. A colour representation of the distribution of $\rho(\alpha^{|}_{\oplus})$ for the neighbourhood of a general material point is shown adjacent to the deformed square.

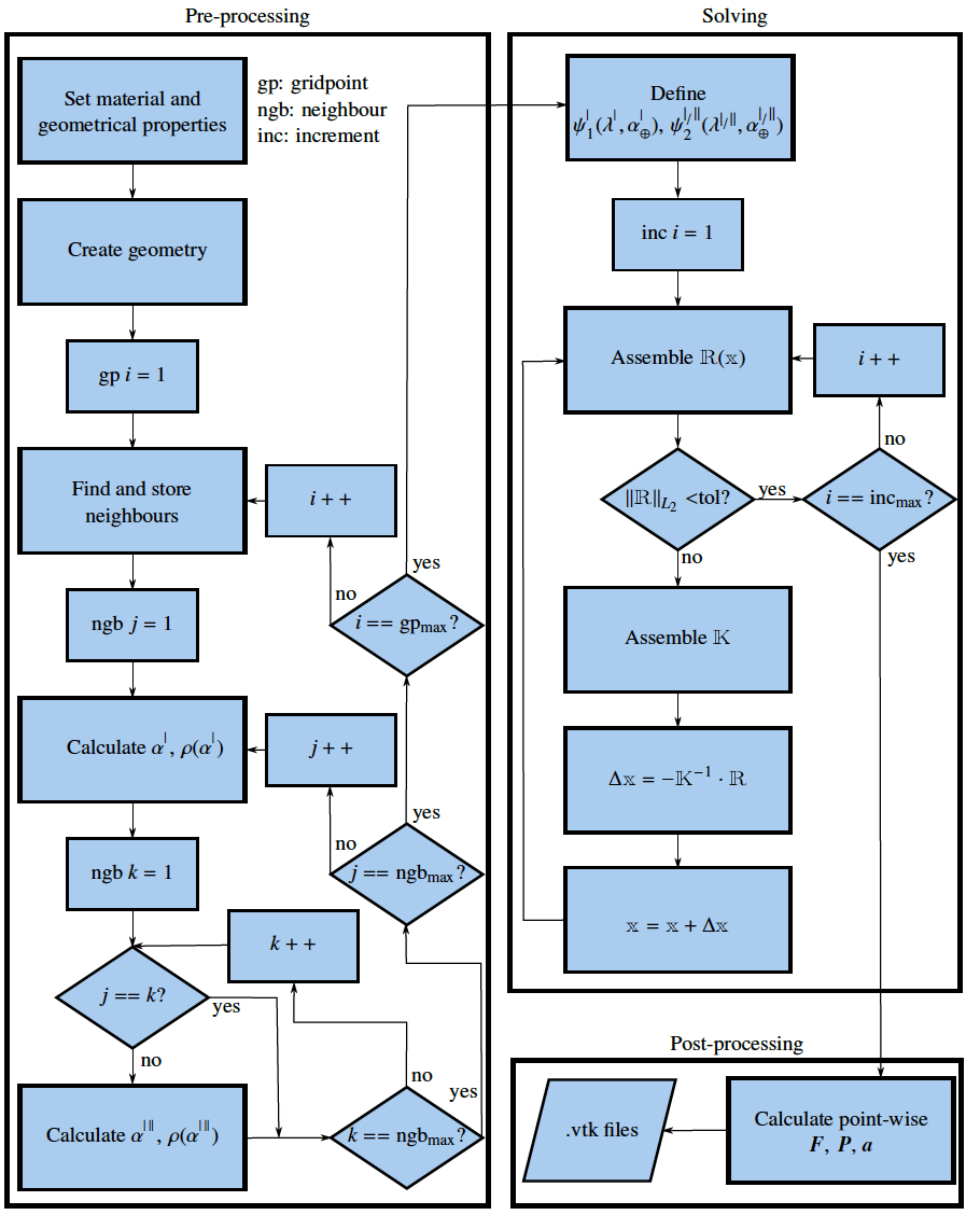

Figure 4: Flowchart illustrating the implementation of the CPD framework with line and area elements.

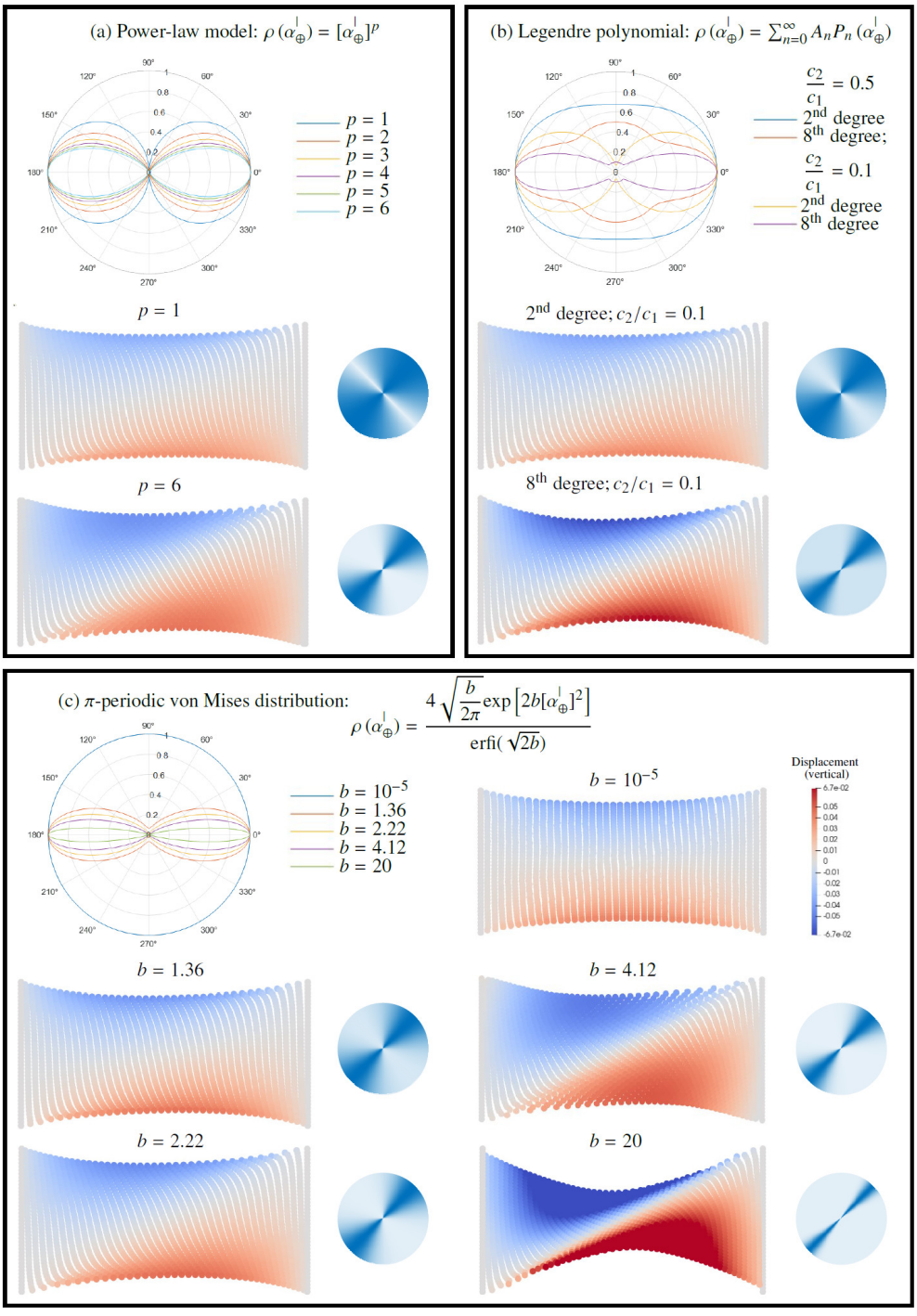

Figure 5: Comparison of results for different forms of $\rho(\alpha_{\oplus}^{|})$. A 100% uniaxial extension of a transversely isotropic square with preferred direction $\boldsymbol{A}$ specified by $\gamma = 45°$. The isotropic and transverse isotropic bond stiffness coefficients are $C_{1,\text{iso}} = 0.01$ and $C_{1,\text{ani}} = 1$, respectively. Each subfigure shows the normalised polar plot of $\rho(\alpha_{\oplus}^{|})$, the displacement in the vertical direction on the deformed square and a colour representation of $\rho(\alpha_{\oplus}^{|})$ on the neighbourhood of general point.

Figure 5 (a) shows the results for a power-law model where

$$\rho\left(\alpha_{\oplus}^{|}\right) = \left[\alpha_{\oplus}^{|}\right]^{p}, \tag{54}$$

for values of the exponent $p > 1$. For this model, there is no resistance in the direction perpendicular to $\boldsymbol{A}$. This can lead to physical instability for high values of p. Isotropic bulk resistance is required to avoid this situation. To circumvent this issue an additive decomposition of potential energies (Eq. 39) is used and the bond stiffness constants are set to $C_{1,\mathrm{ani}} = 1$ and $C_{1,\mathrm{iso}} = 0.01$.

Figure 5 (b) shows the results when using Legendre polynomials for $\rho\left(\alpha_{\oplus}^{|}\right)$, as suggested by Ghajari et al. (2014), where

$$\rho\left(\alpha_{\oplus}^{|}\right) = \sum_{n=0}^{\infty} A_n P_n\left(\alpha_{\oplus}^{|}\right). \tag{55}$$

Here n denotes the degree of the polynomial, A_n the associated polynomial coefficient, and P_n the associated Legendre functions. In order to fully determine $\rho\left(\alpha_{\oplus}^{|}\right)$ its value at five different angles should be specified. In the model proposed by Ghajari et al. (2014), two parameters, c_1 and c_2 are used and $\rho\left(1\right) = c_1,\ \rho(\alpha_{\oplus}^{|}) = c_2$ for $\cos^{-1}(\alpha_{\oplus}^{|}) = 45°,\ 55°,\ 65°,$ and $90°$. Results for a ratio of $c_2/c_1 = 0.1$ for the second and eighth degree Legendre polynomials are shown in Figure 5. For these cases, c_2 can be interpreted as an isotropic contribution to the resistance. This cannot however be generalised for arbitrary choices of the degree of the polynomial.

Histological data of fibrous biological tissue, such as experimentally determined collagen fibre distributions, are often modelled by a von Mises distribution (Gasser et al., 2006). The form of the scaling function based on the dispersion of fibres, expressed by the concentration parameter b, is given by

$$\rho\left(\alpha_{\oplus}^{|}\right) = \frac{4\sqrt{\frac{b}{2\pi}}\exp\left[2b[\alpha_{\oplus}^{|}]^2\right]}{\mathrm{erfi}(\sqrt{2b})}. \tag{56}$$

This choice of scaling function can represent an isotropic material ($b \approx 0$), fully aligned fibres ($b \to \infty$), and scenarios in between. Figure 5 (c) shows the resulting displacements for different choices of b. Note that as b increases, i.e., the fibres become more aligned, the model becomes physically unstable if there is no bulk resistance to confer stability to the material. To avoid this, the bond stiffness constants are set to $C_{1,\mathrm{ani}} = 1$ and $C_{1,\mathrm{iso}} = 0.01$.

6.1.2. ρ as an influence function

Choosing $\rho = \rho\left(\alpha_{\oplus}^{|}; \Xi^{|}\right)$ introduces a dependence on the distance $\Xi^{|}$ between the two points in the sense of a parametrisation (as indicated by the semicolon notation). The density function therefore resembles an influence function and determines which of the neighbours contributes to the energy and $C_{1,\mathrm{ani}} = \rho\left(\alpha_{\oplus}^{|}; \Xi^{|}\right) C_1$. This choice corresponds to the proposal by Ahadi and Krochmal (2018). A general form for an influence function is given by

$$\rho\left(\alpha_{\oplus}^{|}; \Xi\right) = \begin{cases} g\left(\alpha_{\oplus}^{|}\right) & \text{if } \Xi^{|} \leq \mathrm{r}\left(\alpha_{\oplus}^{|}\right), \\ 0 & \text{otherwise}. \end{cases} \tag{57}$$

For the simplest case, the function $g\left(\alpha_{\oplus}^{|}\right) = 1$ and a neighbour either contributes fully to the energy or it does not contribute at all. The simplest version of the scalar measure $r\left(\alpha_{\oplus}^{|}\right)$ would be the radius of a circle. Figure 6 shows the

deformation of an initially unit square subjected to 100% uniaxial extension for the choice of an elliptical $r(\alpha^{|}_{\oplus})$ with a horizontal long axis. The eccentricity

$$e = \sqrt{1 - \left(\frac{r_{\min}}{\delta_0}\right)^2}, \tag{58}$$

describes the ratio of the lengths of the principal axes of the ellipse, where $r_{\min}$ denotes the minor axis length. The square domain has a fixed fibre orientation ($\gamma = 45°$), and the investigation is limited to the case where $g(\alpha^{|}_{\oplus}) = 1$, $C_{1,\text{ani}} = 1$, and $C_{1,\text{iso}} = 0.01$. The polar plots show the shape of $r(\alpha^{|}_{\oplus})$. As the eccentricity increases, the results more closely resemble those of the fully-aligned fibre.

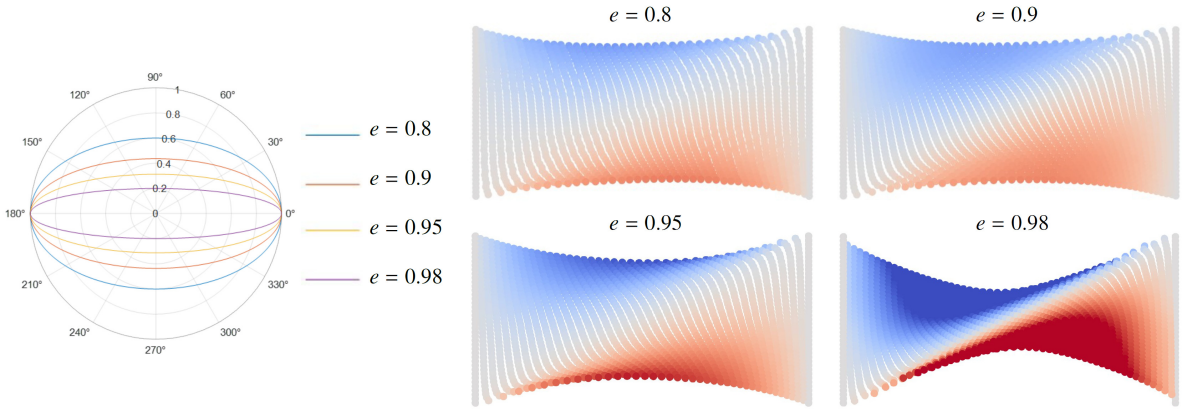

Figure 6: Comparison of results when ρ is considered as an influence function. A 100% uniaxial extension of a transversely isotropic square with $\gamma = 45°$ defined anti-clockwise from the horizontal. Showing the deformation of an elliptical $r(\alpha^{|}_{\oplus})$ with $g(\alpha^{|}_{\oplus}) = 1$. The polar plot shows the shape of $r(\alpha^{|}_{\oplus})$. The isotropic and transverse isotropic bond stiffness coefficients are $C_{1,\text{iso}} = 0.01$ and $C_{1,\text{ani}} = 1$, respectively.

6.1.3. Prescribing the preferred direction

Figure 7 shows the effect that varying the preferred direction has on the deformation of a unit square subjected to 100% uniaxial extension using the von Mises distribution model for $\rho(\alpha^{|}_{\oplus})$ and $b = 4.12$.

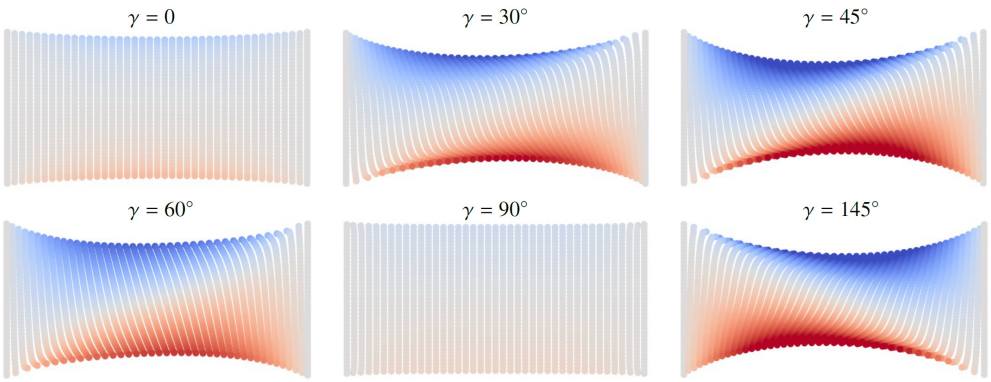

Figure 7: A unit square subjected to 100% uniaxial tension for various values of γ. The deformed body is coloured according to its vertical displacement.

6.1.4. *The interplay between the isotropic and anisotropic contribution*

The impact of the choice of $C_{1,\text{ani}}$ and $C_{1,\text{iso}}$ on the unit square subjected to 100% uniaxial tension is shown in Figure 8. Two options for $\rho\left(\alpha^{|}_{\oplus}\right)$ in Eq. (56), obtained by setting $b = 4.12$ and $b = 20$, are examined. The difference in the deformation for the two values of b becomes more pronounced as the stiffness in the preferred direction increases.

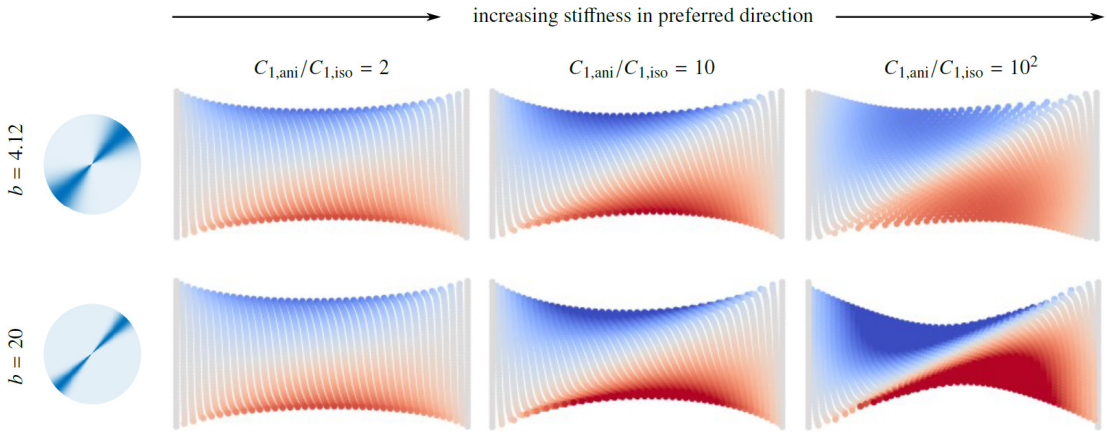

Figure 8: The influence of increasing the stiffness in the preferred direction. Large deformation of a unit square with $b = 4.12$ and $b = 20$ using the von Mises distribution model for $\rho\left(\alpha^{|}_{\oplus}\right)$ and $\gamma = 45°$. An increasing ratio of $C_{1,\text{ani}}/C_{1,\text{iso}}$ from left to right is shown.

6.1.5. *Other modes of deformation*

The versatility of the proposed model is highlighted by comparing the deformation of a square subjected to 50% simple shear. Figure 9 shows the vertical displacement for different prescribed values of the fibre orientation angle γ.

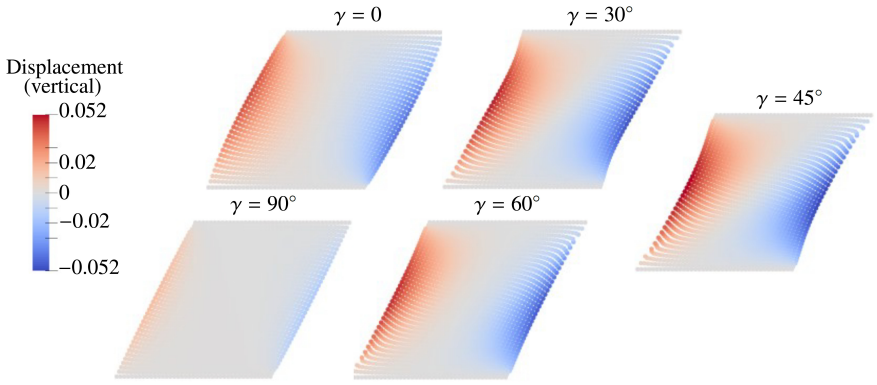

Figure 9: A unit square subjected to shear using the von Mises distribution model for $\rho\left(\alpha^{|}_{\oplus}\right)$ with $b = 4.12$ and various choices of γ.

6.2. *Multi-neighbour interactions, with transverse isotropy only included in line element interactions*

In Section 6.1 only the energy contributions associated with line element interactions for both the isotropic and anisotropic contributions were considered. The harmonic isotropic potential energy triple- and quadruple-densities for area and volume elements, respectively, analogous to Eq. (51), are given by

$$\psi^{|/\shortparallel}_{2,\text{iso}}(\lambda^{|/\shortparallel}) = \frac{1}{2} C_{2,\text{iso}}\, \boldsymbol{\Xi}^{|/\shortparallel}\, [\lambda^{|/\shortparallel} - 1]^2 \qquad \text{and} \qquad \psi^{|/\shortparallel/\shortparallel\shortparallel}_{3,\text{iso}}(\lambda^{|/\shortparallel/\shortparallel\shortparallel}) = \frac{1}{2} C_{3,\text{iso}}\, \boldsymbol{\Xi}^{|/\shortparallel/\shortparallel\shortparallel}\, [\lambda^{|/\shortparallel/\shortparallel\shortparallel} - 1]^2 \,. \tag{59}$$

6.2.1. *Compressibility*

Figure 10 illustrates the interplay between $C_{1,\text{iso}}, C_{2,\text{iso}}$, and $C_{1,\text{ani}}$ for a square domain subjected to 100% uniaxial extension. The von Mises distribution model for $\rho\,(\alpha^{|}_{\oplus})$ with $b = 2.22$ is used. As the ratio of $C_{2,\text{iso}}/C_{1,\text{iso}}$ increases from the top to the bottom of the tabulated figure, the material becomes less compressible, i.e., it exhibits a more incompressible response, resulting in a thinner cross-section (see also Javili et al. (2020)). As the ratio of $C_{1,\text{ani}}/C_{1,\text{iso}}$ increases, the material resists deformation along the preferred diagonal direction (i.e., $\gamma = 45°$) and consequently opposes the thinning of the cross-section. The shape of the deformed square depends on the material properties i.e., which of the competing physical phenomena dominates.

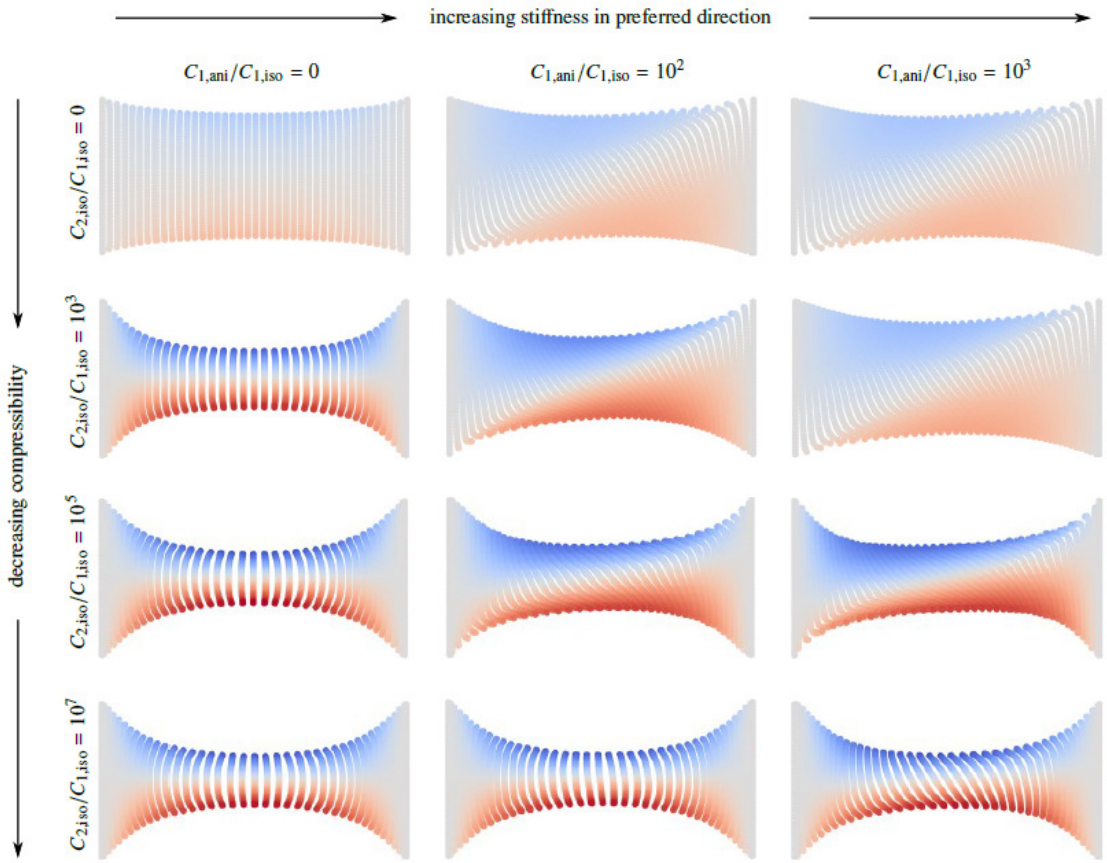

Figure 10: The influence of varying compressibility and stiffness in the preferred direction. Large deformations of a unit square with a preferred direction specified by $\gamma = 45°$ using the von Mises distribution model for $\rho(\alpha^{|}_{\oplus})$ with $b = 2.22$. Showing increasing ratio's of $C_{1,\text{ani}}/C_{1,\text{iso}}$ from left to right and increasing ratio's of $C_{2,\text{iso}}/C_{1,\text{iso}}$ from top to bottom.

6.2.2. *Block reinforced by two families of fibres*

The following example is motivated by a local model of the transverse isotropic response of biological tissue and involves the imposition of simple tension to iliac adventitial strips (Gasser et al., 2006). The dimensions of the strip are $4 \times 2 \times 0.5$. Note that the example does not intend to reproduce the test case, but rather to illustrate that the proposed model can capture the key characteristic behaviour. The material is nearly incompressible ($C_3 = 10^5$), mimicking the incompressibility of biological tissue. Two preferred directions are prescribed, with $\gamma = 49.98°$ being

the axial direction and $\gamma = 40.02°$ the circumferential direction. The von Mises distribution used for $\rho\,(\alpha^{|}_{\oplus})$ captures the dispersion of the fibres associated with collagen distribution and is informed by the local version in (Gasser et al., 2006). The two values assigned to the concentration parameter, $b = 100$ and $b = 1.36$, correspond to the values used for the dispersion parameter in (Gasser et al., 2006), mimicking fully-aligned fibres and fibres with some dispersion, respectively. The ratio of the relative stiffness of the preferred direction to the bulk of the strip is high at $(C_{1,\text{ani}}/C_{1,\text{iso}} = 10^3)$. Uniaxial extensions of 50% and 28% in the circumferential and axial directions, respectively, are prescribed. There are differences between the current example and Gasser et al. (2006): the energy density for both the isotropic and preferred direction is different; a Dirichlet boundary condition is used here; PD is a non-local formulation necessitating a thicker body to circumvent issues stemming from boundary effects. Thus, this is a qualitative and not a quantitative comparison.

Figure 11 shows the component of the Cauchy stress tensor in the direction of extension (determined as outlined below) superimposed upon the deformed configuration. The results for including dispersion of the fibres and for fully aligned fibres are shown for both the circumferential and axial specimens. The results correspond well to the test case. In order to calculate the Cauchy stress, the effective deformation gradient $\boldsymbol{F}$ is first calculated (Silling et al., 2007) as

$$\boldsymbol{F} = \left[\int_{\mathcal{H}_0} \boldsymbol{E}^{|} \otimes \boldsymbol{E}^{|}\, \mathrm{d}V^{|}\right]^{-1} \cdot \int_{\mathcal{H}_0} \frac{1}{\Xi^{|}}\, \boldsymbol{\xi}^{|} \otimes \boldsymbol{E}^{|}\, \mathrm{d}V^{|}\,. \tag{60}$$

The effective Cauchy stress $\boldsymbol{\sigma}$ is then calculated using the effective Piola stress tensor $\boldsymbol{P}$ as follows

$$\boldsymbol{\sigma} = \frac{1}{J}\boldsymbol{P}\cdot\boldsymbol{F}^T \quad \text{with} \quad J = \det\boldsymbol{F} \quad \text{and} \quad \boldsymbol{P} = \int_{\mathcal{H}_0} \boldsymbol{p}^{|} \otimes \boldsymbol{\Xi}^{|}\, \mathrm{d}V^{|}. \tag{61}$$

Figure 12 shows the prediction of the deformed collagen fibre orientations, i.e., $\boldsymbol{a}_i = \boldsymbol{F}\cdot\boldsymbol{A}_i$ for $i = 1, 2$. The orientation measure $c_{\boldsymbol{a}} = \boldsymbol{a}_1 \cdot \boldsymbol{a}_2$ corresponds well with the benchmark example.

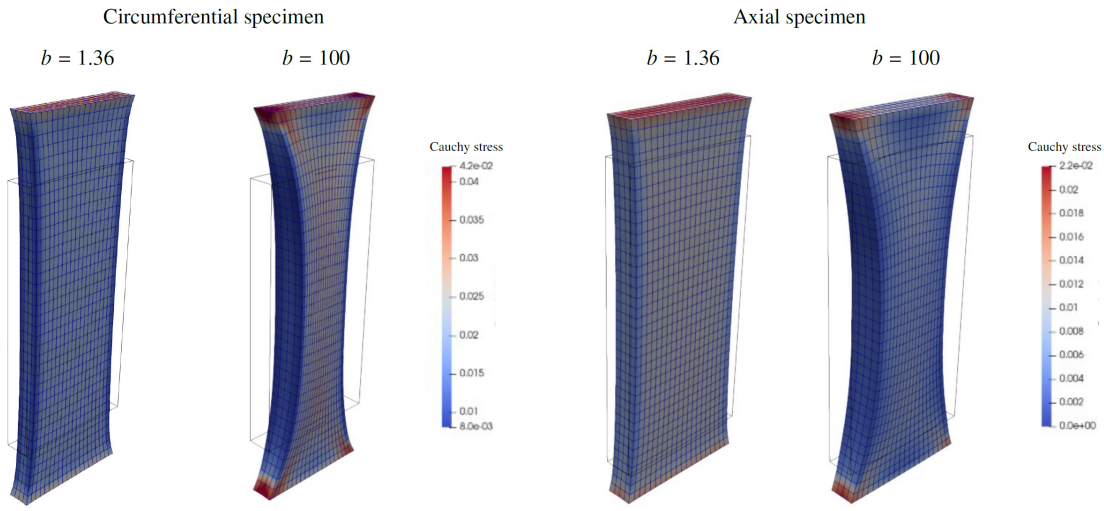

Figure 11: Fibre reinforced blocks resembling a circumferential and an axial specimen of a iliac adventitial strip, subjected to uniaxial extension of 50% and 28%, respectively. The Cauchy stress in the direction of the applied load is plotted. The cases on the left correspond to dispersion in the collagen fibres, and on the right to no dispersion (fully aligned fibres).

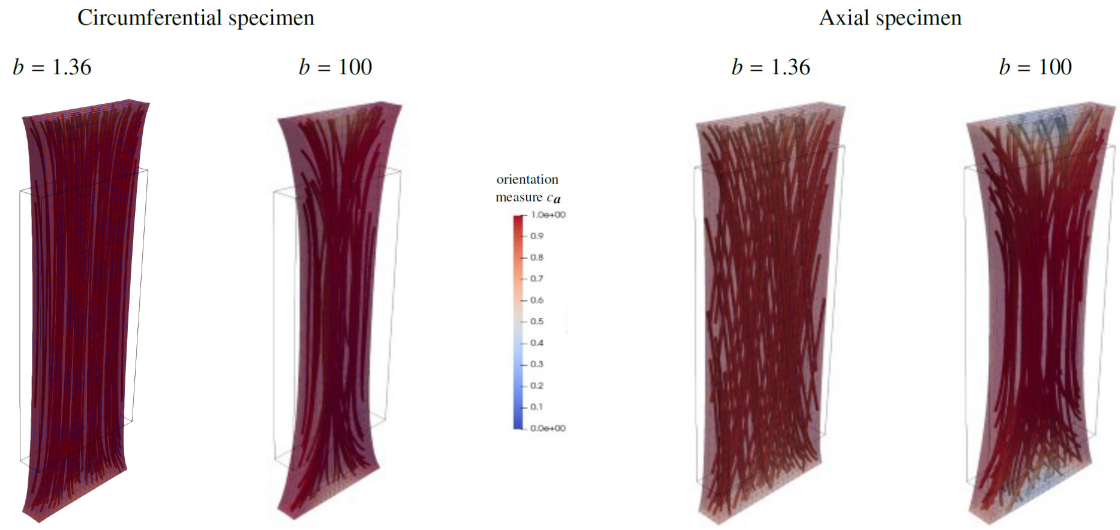

Figure 12: Prediction of the current (mean) collagen orientations using the orientation measure $c_{\boldsymbol{a}} = \boldsymbol{a}_1 \cdot \boldsymbol{a}_2$. Results are shown for circumferential and axial specimens. The cases on the left correspond to dispersion in the collagen fibres, and on the right to no dispersion (fully aligned fibres).

6.3. Transverse isotropy extended to area element interactions

The model for transverse isotropy incorporating only line elements (see Section 3.1) is now compared to that for area elements (Section 3.2). The general format for the harmonic transversely isotropic potential energy triple-density that ensures that the material configuration is in equilibrium for zero deformation is given by

$$\psi^{|/\!/|}_{2,\mathrm{ani}}(\lambda^{|/\!/|}, \alpha^{|/\!/|}_{\oplus}) = \frac{1}{2} C_{2,\mathrm{ani}}\, \rho\,(\alpha^{|/\!/|}_{\oplus})\; \boldsymbol{\Xi}^{|/\!/|}\, [\lambda^{|/\!/|} - 1]^2 \,. \tag{62}$$

Consider a fibre-reinforced cube with a 40% cuboid cutout subjected to uniform expansion as shown in Figure 13. The fibres are oriented diagonally as shown in the top right of the figure. The dimensions of the cube are $2 \times 2 \times 2$ and a grid spacing of $\Delta = 0.1$ is used along with a ratio of $\delta/\Delta = 2$. The stiffness for the bulk material is $C_{1,\mathrm{iso}} = 1$ and the stiffness of the fibres is $C_{1,\mathrm{ani}} = 10^3$ and $C_{2,\mathrm{ani}} = 10^6$ for the line and area element interactions, respectively. A von Mises distribution model was used to describe the fibres with $b = 4.12$. The results obtained using line element transverse isotropy are shown on the left and those from area element transverse isotropy are shown on the right. The deformation of the cutout on planes along the fibre direction and orthogonal to the fibre direction are highlighted at the bottom of the figure for both line and area element transverse isotropy. Deformation along the direction of the fibre is resisted in the material for line element transverse isotropy, resulting in a elongated cutout. For area element transverse isotropy, the resistance is orthogonal to the fibre direction, resulting in a rounded cutout on the orthogonal plane. The convergence of the Newton–Raphson scheme employed to solve the discrete form of the nonlinear governing equations is quadratic as indicated in Table 1.

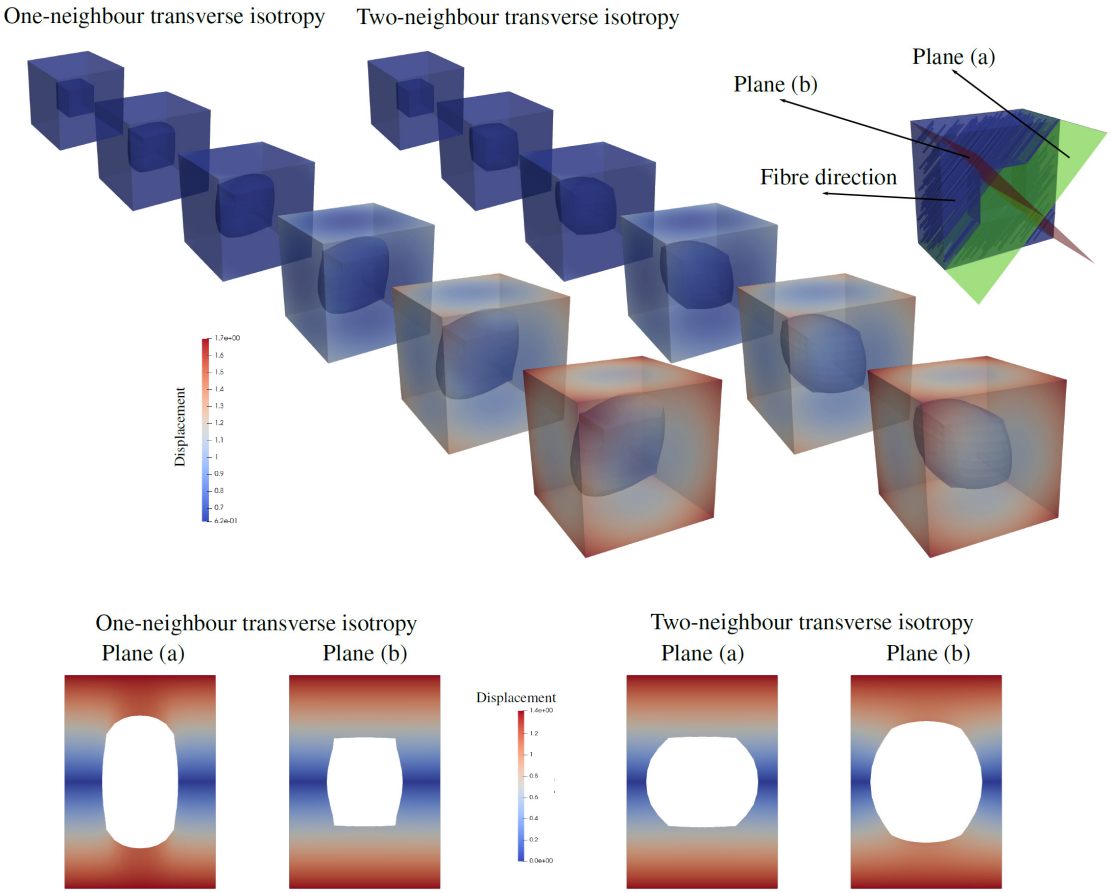

Figure 13: Comparison between one-neighbour and two-neighbour anisotropy. The block with cutout is expanded uniformly. Fibres are aligned diagonally through block. Plane (b) is orthogonal to the direction of the fibres, and Plane (a) is one of the orthogonal planes to Plane (b), as shown.

Increment (deformation)				
2 (20%)	4 (40%)	6 (60%)	8 (80%)	10 (100%)
One-neighbour transverse isotropy				
1.00e+00	1.00e+00	1.00e+00	1.00e+00	1.00e+00
4.19e-02	4.15e-02	3.35e-02	2.68e-02	2.16e-02
3.68e-03	2.05e-03	1.38e-03	7.20e-04	3.52e-04
2.56e-06	6.92e-07	2.92e-07	6.23e-08	1.10e-08
2.58e-11	1.11e-12	1.71e-13	8.83e-14	1.01e-13
4.62e-14	6.37e-14			
Two-neighbour transverse isotropy				
1.00e+00	1.00e+00	1.00e+00	1.00e+00	1.00e+00
5.38E-02	5.75E-02	6.10E-02	6.38E-02	6.16E-02
2.58E-04	1.40E-04	1.15E-04	1.36E-04	1.32E-04
1.13E-08	2.63E-09	1.57E-09	1.19E-09	1.43E-09
4.46E-14	6.78E-14	7.04E-14	7.22E-14	8.24E-14

Table 1: $L2$-norm of the residual for one neighbour interactions and two-neighbour interactions respectively, showing the quadratic convergence of the Newton–Raphson solver.

6.4. Relation to classical linear elasticity

One-neighbour interactions are an example of central interactions, with research on this topic dating back to the work by Cauchy in his fundamental account on elasticity. Central interactions result in well-known constraints on the material parameters in the continuum modelling of elasticity. For geometrically linear elasticity in CCM these result in the so-called Cauchy relations allowing for the exchange of the two middle indices of the fourth-order elasticity tensor $C_{ijkl} = C_{ikjl}$. As a consequence, for central interactions the number of independent material parameters in the elasticity tensor reduces from 21 to 15 for general anisotropy, from 5 to 3 for transverse isotropy, and from 2 to 1 for isotropy (Itin, 2024; Trageser and Seleson, 2020). It has been shown that for affine and linearized deformations in the case of isotropic peridynamics when only one-neighbour interactions are considered, a linear elasticity correspondence model, (i.e., CCM) with the constraint of equal Lamé constants, $\mu = \lambda$, and thus a Poisson ratio of $1/4$ results (Ekiz et al., 2022a,b). Taking multi-neighbour interactions into account allows for the spanning of the entire allowable range of Poisson ratios $(-1, 1/2)$ for the linear elasticity correspondence model of isotropic CPD.
In the following section the independent material parameters of both one-neighbour and multi-neighbour interactions for transverse isotropy will be explored.

6.4.1. Solely line element interactions

For CPD, we can obtain the point-wise energy density for line element interactions from Eq. (52) by integrating over the horizon as

$$\psi_{1,\text{ani}} = \frac{C_{1,\text{ani}}}{2} \int_{\mathcal{H}_0} \rho\,(\alpha_{\oplus}^{|})\, \Xi^{|}\, [\varepsilon^{|}]^2 \,\mathrm{d}V^{|}, \tag{63}$$

where $\varepsilon^{|} := \lambda^{|} - 1$ denotes the strain of a line element. Note that CPD is a formulation directly formulated for large-deformations, thus to compare the independent material parameters to those from linear transverse isotropy, $\psi_{1,\text{ani}}$ should be evaluated at small deformations, and henceforth denoted as $\psi^{\varepsilon}_{1,\text{ani}}$. Thus, we first linearize the strain measure of the energy density, via the generic linearization operator defined by

$$\mathcal{L}\{\bullet\} = \{\bullet\}\big|_{\boldsymbol{F}=\boldsymbol{I}} + \frac{\partial}{\partial \boldsymbol{F}}(\{\bullet\})\big|_{\boldsymbol{F}=\boldsymbol{I}} : [\boldsymbol{F} - \boldsymbol{I}]\,. \tag{64}$$

After some mathematical steps that we omit here for the sake of brevity we arrive at

$$\mathcal{L}\varepsilon^{|} = \boldsymbol{I}^{|} : \boldsymbol{\varepsilon} \quad \text{with} \quad \boldsymbol{I}^{|} := \boldsymbol{E}^{|} \otimes \boldsymbol{E}^{|} \quad \text{and} \quad \boldsymbol{\varepsilon} = [\boldsymbol{F} - \boldsymbol{I}]^{\text{sym}}\,, \tag{65}$$

where $\boldsymbol{\varepsilon}$ is the familiar small strain tensor, also known as the Cauchy strain tensor. Equipped with the linearized strain measure of CPD, we can now write the point-wise quadratic strain energy density in terms of $\boldsymbol{\varepsilon}$ and the fourth order elasticity tensor associated with line elements $\mathbb{E}_{1,\text{ani}}$ as

$$\psi^{\varepsilon}_{1,\text{ani}} = \frac{1}{2}\,\boldsymbol{\varepsilon} : \mathbb{E}_{1,\text{ani}} : \boldsymbol{\varepsilon} \quad \text{with} \quad \mathbb{E}_{1,\text{ani}} = C_{1,\text{ani}}\,\mathbb{C}_{1,\text{ani}}, \tag{66}$$

with the normalised elasticity tensor associated with line elements $\mathbb{C}_{1,\text{ani}}$ given by:

$$\mathbb{C}_{1,\text{ani}} = \int_{\mathcal{H}_0} \rho\,(\alpha_{\oplus}^{|})\, \Xi^{|}\, \mathbb{I}^{|} \mathrm{d}V^{|} \quad \text{where} \quad \mathbb{I}^{|} = \boldsymbol{E}^{|} \otimes \boldsymbol{E}^{|} \otimes \boldsymbol{E}^{|} \otimes \boldsymbol{E}^{|}. \tag{67}$$

Restricting attention to a spherical horizon and conveniently specifying $\boldsymbol{A} = \boldsymbol{E}_3$, the unit vectors can be expressed in spherical coordinates as $\boldsymbol{E}^{\shortmid} \hat{=} \left[\sin\phi^{\shortmid}\cos\theta^{\shortmid},\, \sin\phi^{\shortmid}\sin\theta^{\shortmid},\, \cos\phi^{\shortmid}\right]$ and the density function by $\rho = \rho\,(|\cos\phi^{\shortmid}|)$. After splitting the integral and integrating with respect to $\Xi^{\shortmid}$, $\mathbb{C}_{1,\mathrm{ani}}$ can be written in terms of the double normalised elasticity tensor $\mathbb{B}_{1,\mathrm{ani}}$:

$$\mathbb{C}_{1,\mathrm{ani}} \approx \delta_0^4\, \mathbb{B}_{1,\mathrm{ani}} \quad \text{with} \quad \mathbb{B}_{1,\mathrm{ani}} = \int_{\theta^{\shortmid}=0}^{\theta^{\shortmid}=2\pi} \int_{\phi^{\shortmid}=0}^{\phi^{\shortmid}=\pi} \mathbb{I}^{\shortmid} \rho\,(|\cos\phi^{\shortmid}|)\sin\phi^{\shortmid}\,\mathrm{d}\phi^{\shortmid}\,\mathrm{d}\theta^{\shortmid}\,. \tag{68}$$

After integration $\mathbb{B}_{1,\mathrm{ani}}$ can be expressed in terms of two isotropy parameters, $a_1^{\shortmid}$ and $a_2^{\shortmid}$ and three transverse isotropy parameters $a_3^{\shortmid} - a_5^{\shortmid}$ in the form:

$$\begin{aligned}\mathbb{B}_{1,\mathrm{ani}} \doteq\ & a_1^{\shortmid}\,[\boldsymbol{I}\otimes\boldsymbol{I}] + a_2^{\shortmid}\left[\boldsymbol{I}\overline{\otimes}\boldsymbol{I} + \boldsymbol{I}\underline{\otimes}\boldsymbol{I}\right] + a_3^{\shortmid}\,[\boldsymbol{A}\otimes\boldsymbol{A}\otimes\boldsymbol{A}\otimes\boldsymbol{A}] \\ & + a_4^{\shortmid}\left[\boldsymbol{I}\overline{\otimes}\,[\boldsymbol{A}\otimes\boldsymbol{A}] + \boldsymbol{I}\underline{\otimes}\,[\boldsymbol{A}\otimes\boldsymbol{A}] + [\boldsymbol{A}\otimes\boldsymbol{A}]\,\overline{\otimes}\boldsymbol{I} + [\boldsymbol{A}\otimes\boldsymbol{A}]\,\underline{\otimes}\boldsymbol{I}\right] + a_5^{\shortmid}\,[\boldsymbol{I}\otimes[\boldsymbol{A}\otimes\boldsymbol{A}] + [\boldsymbol{A}\otimes\boldsymbol{A}]\otimes\boldsymbol{I}]\,.\end{aligned} \tag{69}$$

By comparing the coefficients of $\mathbb{B}_{1,\mathrm{ani}}$ in terms of $a_1^{\shortmid} - a_5^{\shortmid}$ with entries obtained from tediously evaluating the integral in Eq. (68) we obtain the following system of linear equations:

$$\begin{bmatrix}1&2&1&4&2\\1&0&0&0&0\\1&0&0&0&1\\0&1&0&0&0\\0&1&0&1&0\end{bmatrix}\begin{bmatrix}a_1^{\shortmid}\\a_2^{\shortmid}\\a_3^{\shortmid}\\a_4^{\shortmid}\\a_5^{\shortmid}\end{bmatrix} \doteq \begin{bmatrix}c_2^{\shortmid}\\c_1^{\shortmid}\\c_3^{\shortmid}\\c_1^{\shortmid}\\c_3^{\shortmid}\end{bmatrix} \quad\Rightarrow\quad \begin{bmatrix}a_1^{\shortmid}\\a_2^{\shortmid}\\a_3^{\shortmid}\\a_4^{\shortmid}\\a_5^{\shortmid}\end{bmatrix} = \begin{bmatrix}c_1^{\shortmid}\\c_1^{\shortmid}\\3c_1^{\shortmid} + c_2^{\shortmid} - 6c_3^{\shortmid}\\-c_1^{\shortmid} + c_3^{\shortmid}\\-c_1^{\shortmid} + c_3^{\shortmid}\end{bmatrix}. \tag{70}$$

Thus, the transverse isotropic fourth-order tensor can be written in terms of new coefficients $c_1^{\shortmid}$, $c_2^{\shortmid}$, $c_3^{\shortmid}$:

$$\begin{aligned}\mathbb{B}_{1,\mathrm{ani}} \doteq\ & c_1^{\shortmid}\left[\boldsymbol{I}\otimes\boldsymbol{I} + \boldsymbol{I}\overline{\otimes}\boldsymbol{I} + \boldsymbol{I}\underline{\otimes}\boldsymbol{I}\right] + \left[3c_1^{\shortmid} + c_2^{\shortmid} - 6c_3^{\shortmid}\right][\boldsymbol{A}\otimes\boldsymbol{A}\otimes\boldsymbol{A}\otimes\boldsymbol{A}] \\ & + \left[c_3^{\shortmid} - c_1^{\shortmid}\right]\left[\boldsymbol{I}\overline{\otimes}\,[\boldsymbol{A}\otimes\boldsymbol{A}] + \boldsymbol{I}\underline{\otimes}\,[\boldsymbol{A}\otimes\boldsymbol{A}] + [\boldsymbol{A}\otimes\boldsymbol{A}]\,\overline{\otimes}\boldsymbol{I} + [\boldsymbol{A}\otimes\boldsymbol{A}]\,\underline{\otimes}\boldsymbol{I} + \boldsymbol{I}\otimes[\boldsymbol{A}\otimes\boldsymbol{A}] + [\boldsymbol{A}\otimes\boldsymbol{A}]\otimes\boldsymbol{I}\right].\end{aligned} \tag{71}$$

Note that for line element interactions only, just one of the two isotropy parameters is independent and only two of the three transverse isotropy parameters are independent. Note that furthermore, the transverse isotropy parameters $a_3^{\shortmid}$ to $a_5^{\shortmid}$ vanish identically for isotropy. Taken together, the Cauchy relations of CCM are retained.

6.4.2. Line and area element interactions

The point-wise energy density associated with area element interactions can be obtained from Eq. (62) by twice integrating over the horizon as

$$\psi_{2,\mathrm{ani}} = \frac{C_{2,\mathrm{ani}}}{2} \int_{\mathcal{H}_0}\int_{\mathcal{H}_0} \rho\,(\alpha_{\oplus}^{|/\shortparallel|})\,\Xi^{|/\shortparallel|}\,[\varepsilon^{|/\shortparallel|}]^2\,\mathrm{d}V^{\shortparallel}\,\mathrm{d}V^{\shortmid}\,, \tag{72}$$

where $\varepsilon^{|/\shortparallel|} := \lambda^{|/\shortparallel|} - 1$ denotes the strain of an area element. The strain measure of the energy density can be linearized, via the generic linearization operator defined in Eq. (64) to arrive , after some mathematical steps, at

$$\mathcal{L}\,\varepsilon^{|/\shortparallel|} = \left[\boldsymbol{I} - \boldsymbol{E}^{|/\shortparallel|}\otimes\boldsymbol{E}^{|/\shortparallel|}\right] : \boldsymbol{\varepsilon} \quad \text{again with} \quad \boldsymbol{\varepsilon} = [\boldsymbol{F} - \boldsymbol{I}]^{\mathrm{sym}}\,. \tag{73}$$

Equipped with the linearized strain measure of (73), we can now write the point-wise strain energy density in terms of $\boldsymbol{\varepsilon}$ and the elasticity tensor associated with area elements $\mathbb{E}_{2,\text{ani}}$:

$$\psi^{\varepsilon}_{2,\text{ani}} = \frac{1}{2}\,\boldsymbol{\varepsilon} \,:\, \mathbb{E}_{2,\text{ani}} \,:\, \boldsymbol{\varepsilon} \quad \text{with} \quad \mathbb{E}_{2,\text{ani}} = C_{2,\text{ani}}\,\mathbb{C}_{2,\text{ani}}, \tag{74}$$

with the normalised elasticity tensor associated with area elements $\mathbb{C}_{2,\text{ani}}$ given by:

$$\mathbb{C}_{2,\text{ani}} = \int_{\mathcal{H}_0}\int_{\mathcal{H}_0} \rho\,(\alpha^{|/\!/|}_{\oplus})\,\Xi^{|/\!/|}\,\mathbb{I}^{|/\!/|}\mathrm{d}V^{/\!/}\,\mathrm{d}V^{|}\,, \quad \text{where} \quad \mathbb{I}^{|/\!/|} :\ = \Big[\boldsymbol{I} - \boldsymbol{E}^{|/\!/|}\otimes\boldsymbol{E}^{|/\!/|}\Big]\otimes\Big[\boldsymbol{I} - \boldsymbol{E}^{|/\!/|}\otimes\boldsymbol{E}^{|/\!/|}\Big]. \tag{75}$$

We again restrict our attention to a spherical horizon of radius δ_0. Let $\boldsymbol{\Xi}^{|} = \Xi^{|}\boldsymbol{E}^{|}$ and $\boldsymbol{\Xi}^{/\!/} = \Xi^{/\!/}\boldsymbol{E}^{/\!/}$ visit every point within and on a δ_0-sphere independently, then their vector product $\boldsymbol{\Xi}^{|/\!/|} := \boldsymbol{\Xi}^{|}\times\boldsymbol{\Xi}^{/\!/} = \Xi^{|/\!/|}\boldsymbol{E}^{|/\!/|}$ visits every point within and on a δ_0^2-sphere $\mu(\Xi^{|/\!/|})$ times. Therefore, $\boldsymbol{\Xi}^{|/\!/|}$ can be expressed as

$$\boldsymbol{\Xi}^{|/\!/|} \hat{=} \Xi^{|/\!/|}\Big[\sin\phi^{|/\!/|}\cos\theta^{|/\!/|},\ \sin\phi^{|/\!/|}\sin\theta^{|/\!/|},\ \cos\phi^{|/\!/|}\Big]\,, \tag{76}$$

and the integral in Eq. (75) can be equivalently expressed by integrating over the ball with $\Xi^{|/\!/|} \in \Big[0, \delta_0^2\Big]$ (taking $\mu(\Xi^{|/\!/|})$ into account), $\phi^{|/\!/|} \in [0,\pi]$ and $\theta^{|/\!/|} \in [0, 2\pi]$. By specifying $\boldsymbol{A} = \boldsymbol{E}_3$, the unit vectors can be expressed in spherical coordinates by $\boldsymbol{E}^{|/\!/|} \hat{=} \Big[\sin\phi^{|/\!/|}\cos\theta^{|/\!/|},\ \sin\phi^{|/\!/|}\sin\theta^{|/\!/|},\ \cos\phi^{|/\!/|}\Big]$ and the density function by $\rho = \rho\,(|\cos\phi^{|/\!/|}|)$. After splitting the integral and integrating with respect to $\Xi^{|/\!/|}$, $\mathbb{C}_{2,\text{ani}}$ can be written in terms of the double normalised elasticity tensor $\mathbb{B}_{2,\text{ani}}$ as

$$\mathbb{C}_{2,\text{ani}} \approx \delta_0^8\,\mathbb{B}_{2,\text{ani}} \quad \text{with} \quad \mathbb{B}_{2,\text{ani}} = \int_{\theta^{|/\!/|}=0}^{\theta^{|/\!/|}=2\pi}\int_{\phi^{|/\!/|}=0}^{\phi^{|/\!/|}=\pi} \mathbb{I}^{|/\!/|}\rho\,(|\cos\phi^{|/\!/|}|)\sin\phi^{|/\!/|}\,\mathrm{d}\phi^{|/\!/|}\,\mathrm{d}\theta^{|/\!/|}\,. \tag{77}$$

After integration $\mathbb{B}_{2,\text{ani}}$ can be written in the same general form as $\mathbb{B}_{1,\text{ani}}$ (in terms of two isotropy parameters and three transverse isotropy parameters) as

$$\begin{aligned}\mathbb{B}_{2,\text{ani}} \doteq\ & a_1{}^{|/\!/|}\,[\boldsymbol{I}\otimes\boldsymbol{I}] + a_2{}^{|/\!/|}\Big[\boldsymbol{I}\,\overline{\otimes}\,\boldsymbol{I} + \boldsymbol{I}\,\underline{\otimes}\,\boldsymbol{I}\Big] + a_3{}^{|/\!/|}\,[\boldsymbol{A}\otimes\boldsymbol{A}\otimes\boldsymbol{A}\otimes\boldsymbol{A}] \\ & + a_4{}^{|/\!/|}\Big[\boldsymbol{I}\,\overline{\otimes}\,[\boldsymbol{A}\otimes\boldsymbol{A}] + \boldsymbol{I}\,\underline{\otimes}\,[\boldsymbol{A}\otimes\boldsymbol{A}] + [\boldsymbol{A}\otimes\boldsymbol{A}]\,\overline{\otimes}\,\boldsymbol{I} + [\boldsymbol{A}\otimes\boldsymbol{A}]\,\underline{\otimes}\,\boldsymbol{I}\Big] + a_5{}^{|/\!/|}\,[\boldsymbol{I}\otimes[\boldsymbol{A}\otimes\boldsymbol{A}] + [\boldsymbol{A}\otimes\boldsymbol{A}]\otimes\boldsymbol{I}]\,.\end{aligned} \tag{78}$$

By comparing the coefficients of $\mathbb{B}_{2,\text{ani}}$ in terms of $a_1{}^{|/\!/|} - a_5{}^{|/\!/|}$ with entries obtained from meticulously evaluating the integral in Eq. (77) we obtain

$$\begin{bmatrix}1&2&1&4&2\\1&0&0&0&0\\1&0&0&0&1\\0&1&0&0&0\\0&1&0&1&0\end{bmatrix}\begin{bmatrix}a_1{}^{|/\!/|}\\a_2{}^{|/\!/|}\\a_3{}^{|/\!/|}\\a_4{}^{|/\!/|}\\a_5{}^{|/\!/|}\end{bmatrix} \doteq \begin{bmatrix}c_2{}^{|/\!/|} + d_1{}^{|/\!/|} - 2d_3{}^{|/\!/|}\\c_1{}^{|/\!/|} + d_1{}^{|/\!/|} - 2d_2{}^{|/\!/|}\\c_3{}^{|/\!/|} + d_1{}^{|/\!/|} - d_3{}^{|/\!/|} - d_2{}^{|/\!/|}\\c_1{}^{|/\!/|}\\c_3{}^{|/\!/|}\end{bmatrix} \quad\Rightarrow\quad \begin{bmatrix}a_1{}^{|/\!/|}\\a_2{}^{|/\!/|}\\a_3{}^{|/\!/|}\\a_4{}^{|/\!/|}\\a_5{}^{|/\!/|}\end{bmatrix} = \begin{bmatrix}c_1{}^{|/\!/|} + d_1{}^{|/\!/|} - 2d_2{}^{|/\!/|}\\c_1{}^{|/\!/|}\\3c_1{}^{|/\!/|} + c_2{}^{|/\!/|} - 6c_3{}^{|/\!/|}\\-c_1{}^{|/\!/|} + c_3{}^{|/\!/|}\\-c_1{}^{|/\!/|} + c_3{}^{|/\!/|} + d_2{}^{|/\!/|} - d_3{}^{|/\!/|}\end{bmatrix}. \tag{79}$$

Thus, the transverse isotropic fourth-order tensor $\mathbb{B}_{2,\text{ani}}$ can be written in terms of coefficients ${c_1}^{\text{l}/\!/\!\text{l}}$, ${c_2}^{\text{l}/\!/\!\text{l}}$, ${c_3}^{\text{l}/\!/\!\text{l}}$ and ${d_1}^{\text{l}/\!/\!\text{l}}$, ${d_2}^{\text{l}/\!/\!\text{l}}$, ${d_3}^{\text{l}/\!/\!\text{l}}$ as

$$\begin{aligned}\mathbb{B}_{2,\text{ani}} \doteq & \left[{c_1}^{\text{l}/\!/\!\text{l}} + {d_1}^{\text{l}/\!/\!\text{l}} - {d_2}^{\text{l}/\!/\!\text{l}}\right][\boldsymbol{I}\otimes\boldsymbol{I}] + {c_1}^{\text{l}/\!/\!\text{l}}\left[\boldsymbol{I}\,\overline{\otimes}\,\boldsymbol{I} + \boldsymbol{I}\underline{\otimes}\boldsymbol{I}\right] + \left[3{c_1}^{\text{l}/\!/\!\text{l}} + {c_2}^{\text{l}/\!/\!\text{l}} - 6{c_3}^{\text{l}/\!/\!\text{l}}\right][\boldsymbol{A}\otimes\boldsymbol{A}\otimes\boldsymbol{A}\otimes\boldsymbol{A}] \\ & + \left[{c_3}^{\text{l}/\!/\!\text{l}} - {c_1}^{\text{l}/\!/\!\text{l}}\right]\left[\boldsymbol{I}\,\overline{\otimes}\,[\boldsymbol{A}\otimes\boldsymbol{A}] + \boldsymbol{I}\underline{\otimes}\,[\boldsymbol{A}\otimes\boldsymbol{A}] + [\boldsymbol{A}\otimes\boldsymbol{A}]\,\overline{\otimes}\,\boldsymbol{I} + [\boldsymbol{A}\otimes\boldsymbol{A}]\,\underline{\otimes}\boldsymbol{I}\right] \\ & + \left[{c_3}^{\text{l}/\!/\!\text{l}} - {c_1}^{\text{l}/\!/\!\text{l}} + {d_2}^{\text{l}/\!/\!\text{l}} - {d_3}^{\text{l}/\!/\!\text{l}}\right][\boldsymbol{I}\otimes[\boldsymbol{A}\otimes\boldsymbol{A}] + [\boldsymbol{A}\otimes\boldsymbol{A}]\otimes\boldsymbol{I}]\ .\end{aligned} \tag{80}$$

Consequently, for area element interactions there are two independent parameters associated with isotropy and three independent parameters associated with transverse isotropy, on the condition that ${d_2}^{\text{l}/\!/\!\text{l}} \neq {d_3}^{\text{l}/\!/\!\text{l}}$. Thus five independent material parameters are present when area element interactions are used in addition to line element interactions. Furthermore, the transverse isotropy parameters ${a_3}^{\text{l}/\!/\!\text{l}}$ to ${a_5}^{\text{l}/\!/\!\text{l}}$ vanish for isotropy (since then also ${d_2}^{\text{l}/\!/\!\text{l}} = {d_3}^{\text{l}/\!/\!\text{l}}$ holds) and two independent isotropy parameters remain. Taken together, the modelling capacities of linear CCM, both for isotropy and transverse isotropy, are fully retained by our approach to CPD.

7. Conclusion

A framework for incorporating transverse isotropy into CPD has been presented. This significant extension has been developed in the spirit of rational mechanics. Spatial objectivity has been ensured by parameterising the energy densities in terms of the invariants of a Cauchy–Green type secant deformation tensor and a structural tensor defining the preferred anisotropy. The anisotropic response can be associated with either line or area elements, with the former providing modified stiffness in the fibre direction and the latter in the direction orthogonal to the fibre. The governing equations of equilibrium have been derived from the stationarity of the energy functional. The balance of angular momentum has also been satisfied. A series of numerical examples that elucidate the proposed theory have been presented. The ability of our model to account for all five independent constants (two associated with isotropy and three associated with transverse isotropy) characterising transverse isotropy in the linearised case when multi-neighbour interactions are used has been demonstrated. For the case of isotropy the three transverse isotropy constants vanish, while the two independent isotropy parameters remain. For central interactions, only one of the two isotropy constants is independent and only two of the three transverse isotropy constants are independent (i.e,, the Cauchy relations from CCM are retained). Taken together, it has been shown that the modelling capabilities and structure of linear CCM, both for isotropy and transverse isotropy, are fully retained in our approach to CPD.

Future work will investigate alternative forms for the energy density to capture biological tissues and other anisotropic materials undergoing finite deformations. Of particular importance is a more in depth analysis, in the spirit of Ekiz et al. (2022a,b), to investigate the relationship between the material constants that characterise the CPD model and the familiar elastic constants from linearised CCM. The extension of the framework to consider visco- and inelastic materials will also be pursued.

8. Acknowledgements

AdV acknowledges support from the National Graduate Academy for Mathematical and Statistical Sciences (Grant number 821) and the University of Southampton for hosting her from April to November 2023. GL acknowledges the financial support of Roche Diabetes Care. PS acknowledges support from the European Research Council (ERC) under the Horizon Europe program (Grant number 101052785, project: SoftFrac)

References

Adkins, J., 1960. Further symmetry relations for transversely isotropic materials. Archive for Rational Mechanics and Analysis 5, 263–274.

Ahadi, A., Krochmal, J., 2018. Anisotropic peridynamic model—formulation and implementation. AIMS Materials Science 5, 742–755.

Asmanoglo, T., Menzel, A., 2017. A multi-field finite element approach for the modelling of fibre-reinforced composites with fibre-bending stiffness. Computer Methods in Applied Mechanics and Engineering 317, 1037–1067.

Bezanson, J., Edelman, A., Karpinski, S., Shah, V.B., 2017. Julia: A fresh approach to numerical computing. SIAM review 59, 65–98.

Billiar, K.L., Sacks, M.S., 1997. A method to quantify the fiber kinematics of planar tissues under biaxial stretch. Journal of Biomechanics 30, 753–756.

Brewer, K.K., Sakai, H., Alencar, A.M., Majumdar, A., Arold, S.P., Lutchen, K.R., Ingenito, E.P., Suki, B., 2003. Lung and alveolar wall elastic and hysteretic behavior in rats: effects of in vivo elastase treatment. J Appl Physiol (1985) 95, 1926–36.

Diana, V., 2023. Anisotropic continuum-molecular models: A unified framework based on pair potentials for elasticity, fracture and diffusion-type problems. Archives of Computational Methods in Engineering 30, 1305–1344.

Ekiz, E., Steinmann, P., Javili, A., 2022a. From two-to three-dimensional continuum-kinematics-inspired peridynamics: more than just another dimension. Mechanics of Materials 173, 104417.

Ekiz, E., Steinmann, P., Javili, A., 2022b. Relationships between the material parameters of continuum-kinematics-inspired peridynamics and isotropic linear elasticity for two-dimensional problems. International Journal of Solids and Structures 238, 111366.

Eringen, A.C., 1972a. Linear theory of nonlocal elasticity and dispersion of plane waves. International Journal of Engineering Science 10, 425–435.

Eringen, A.C., 1972b. Nonlocal polar elastic continua. International Journal of Engineering Science 10, 1–16.

Eringen, A.C., 1976. Nonlocal micropolar field theory, in: Eringen, A.C. (Ed.), Continuum Physics. Academic Press, New York. volume 4, pp. 205–267.

Eringen, A.C., Edelen, D.G., 1972. On nonlocal elasticity. International Journal of Engineering Science 10, 233–248.

Eringen, A.C., Suhubi, E.S., 1964. Nonlinear theory of simple micro-elastic solids—i. International Journal of Engineering Science 2, 189–203.

Firooz, S., Javili, A., Steinmann, P., 2024. A versatile implicit computational framework for continuum-kinematics-inspired peridynamics. Computational Mechanics 73, 1371–1399.

Fu, Y.B., Ogden, R.W., 2001. Nonlinear Elasticity: Theory and Applications. volume 283 of *London Mathematical Society Lecture Note Series*. Cambridge University Press, Cambridge.

Fung, Y.C., 1993. Biomechanics: Mechanical Properties of Living Tissues. 2nd ed., Springer, New York.

Gasser, T.C., Ogden, R.W., Holzapfel, G.A., 2006. Hyperelastic modelling of arterial layers with distributed collagen fibre orientations. Journal of the royal society interface 3, 15–35.

Ghajari, M., Iannucci, L., Curtis, P., 2014. A peridynamic material model for the analysis of dynamic crack propagation in orthotropic media. Computer Methods in Applied Mechanics and Engineering 276, 431–452.

Gutkin, M., Aifantis, E., 1996. Screw dislocation in gradient elasticity. Scripta Materialia 35, 1353–1358.

Hepworth, D., Steven-Fountain, A., Bruce, D., Vincent, J., 2001. Affine versus non-affine deformation in soft biological tissues, measured by the reorientation and stretching of collagen fibres through the thickness of compressed porcine skin. Journal of biomechanics 34, 341–346.

Holzapfel, G.A., 2000. Nonlinear Solid Mechanics: A Continuum Approach for Engineering. John Wiley & Sons, Chichester, England.

Holzapfel, G.A., Gasser, T.C., Ogden, R.W., 2000. A new constitutive framework for arterial wall mechanics and a comparative study of material models. Journal of elasticity and the physical science of solids 61, 1–48.

Hu, W., Ha, Y.D., Bobaru, F., 2011. Modeling dynamic fracture and damage in a fiber-reinforced composite lamina with peridynamics. International Journal for Multiscale Computational Engineering 9.

Hu, W., Ha, Y.D., Bobaru, F., 2012. Peridynamic model for dynamic fracture in unidirectional fiber-reinforced composites. Computer Methods in Applied Mechanics and Engineering 217, 247–261.

Itin, Y., 2024. Cauchy relations in linear elasticity: Algebraic and physics aspects. Journal of Elasticity 156, 39–77.

Javili, A., Firooz, S., McBride, A.T., Steinmann, P., 2020. The computational framework for continuum-kinematics-inspired peridynamics. Computational Mechanics 66, 795–824.

Javili, A., McBride, A., Mergheim, J., Steinmann, P., 2021a. Towards elasto-plastic continuum-kinematics-inspired peridynamics. Computer Methods in Applied Mechanics and Engineering 380, 113809.

Javili, A., McBride, A., Steinmann, P., 2019a. Continuum-kinematics-inspired peridynamics. Mechanical problems. Journal of the Mechanics and Physics of Solids 131, 125–146.

Javili, A., McBride, A.T., Steinmann, P., 2021b. A geometrically exact formulation of peridynamics. Theoretical and Applied Fracture Mechanics 111, 102850.

Javili, A., Morasata, R., Oterkus, E., Oterkus, S., 2019b. Peridynamics review. Mathematics and Mechanics of Solids 24, 3714–3739.

Krasny, W., Morin, C., Magoariec, H., Avril, S., 2017. A comprehensive study of layer-specific morphological changes in the microstructure of carotid arteries under uniaxial load. Acta Biomaterialia 57, 342–351.

Kröner, E., 1967. Elasticity theory of materials with long range cohesive forces. International Journal of Solids and Structures 3, 731–742.

Laurien, M., Javili, A., Steinmann, P., 2024. Nonlocal interfaces accounting for progressive damage within continuum-kinematics-inspired peridynamics. International Journal of Solids and Structures 290, 112641.

Li, Z., Lu, Y., Huang, D., Rabczuk, T., 2024. Nonlocal anisotropic model for deformation and fracture using peridynamic operator method. Int. J. Mech. Sci. 268, 109023.

Mindlin, R.D., 1964. Micro-structure in linear elasticity. Archive for Rational Mechanics and Analysis 16, 51–78.

Prakash, N., 2022. A general numerical method to model anisotropy in discretized bond-based peridynamics. Journal of Peridynamics and Nonlocal Modeling 4, 257–302.

Rogula, D., 1982. Introduction to nonlocal theory of material media, in: Rogula, D. (Ed.), Nonlocal Theory of Material Media. Springer, Berlin, pp. 125–222.

Scabbia, F., Zaccariotto, M., Galvanetto, U., 2024. A general ordinary state-based peridynamic formulation for anisotropic materials. Computer Methods in Applied Mechanics and Engineering 427, 117059.

Screen, H.R.C., Lee, D.A., Bader, D.L., Shelton, J.C., 2004. An investigation into the effects of the hierarchical structure of tendon fascicles on micromechanical properties. Proceedings of the Institution of Mechanical Engineers. Part H, Journal of engineering in medicine 218, 109–119.

Silling, S.A., 2000. Reformulation of elasticity theory for discontinuities and long-range forces. Journal of the Mechanics and Physics of Solids 48, 175–209.

Silling, S.A., Epton, M., Weckner, O., Xu, J., Askari, E., 2007. Peridynamic states and constitutive modeling. Journal of elasticity 88, 151–184.

Smith, G., Rivlin, R.S., 1957. The anisotropic tensors. Quarterly of Applied Mathematics 15, 308–314.

Spencer, A.J., 1984. Constitutive theory for strongly anisotropic solids, in: Continuum theory of the mechanics of fibre-reinforced composites. Springer, pp. 1–32.

Spencer, A.J.M., Soldatos, K.P., 2007. Finite deformations of fibre-reinforced elastic solids with fibre bending stiffness. International Journal of Non-Linear Mechanics 42, 355–368.

Steigmann, D.J., 2012. Theory of elastic solids reinforced with fibers resistant to extension, flexure and twist. International Journal of Non-Linear Mechanics 47, 734–742.

Steinmann, P., de Villiers, A., McBride, A., Javili, A., 2023. Configurational peridynamics. Mechanics of Materials 185, 104751.

Suhubi, E.S., Eringen, A.C., 1964. Nonlinear theory of micro-elastic solids—ii. International Journal of Engineering Science 2, 389–404.

Tian, D.L., Zhou, X.P., 2021. A continuum-kinematics-inspired peridynamic model of anisotropic continua: Elasticity, damage, and fracture. International Journal of Mechanical Sciences 199, 106413.

Tower, T.T., Neidert, M.R., Tranquillo, R.T., 2002. Fiber alignment imaging during mechanical testing of soft tissues. Annals of Biomedical Engineering 30, 1221–1233.

Trageser, J., Seleson, P., 2020. Bond-based peridynamics: A tale of two poisson's ratios. Journal of Peridynamics and Nonlocal Modeling 2, 278–288.

Vardoulakis, I., Exadaktylos, G., Aifantis, E., 1996. Gradient elasticity with surface energy: mode iii crack problem. International Journal of Solids and Structures 33, 4531–4559.

Wang, C.C., 1970. A new representation theorem for isotropic functions: An answer to professor gf smith's criticism of my papers on representations for isotropic functions: Part 1. scalar-valued isotropic functions. Archive for rational mechanics and analysis 36, 166–197.

Yang, S., Zheng, G., Xia, Y., Shen, G., 2024. A 3d peridynamic model for fracture analysis of transversely isotropic solids. Engineering Fracture Mechanics 297, 109872.

Zheng, Q.S., 1994. Theory of representations for tensor functions—a unified invariant approach to constitutive equations. Applied Mechanics Reviews .

Declaration of interests

☒The authors declare that they have no known competing financial interests or personal relationships that could have appeared to influence the work reported in this paper.

☐The authors declare the following financial interests/personal relationships which may be considered as potential competing interests: